

## Article

# Fabrication of Gelatin Nanofibers by Electrospinning—Mixture of Gelatin and Polyvinyl Alcohol

Hsiu Yu Chi <sup>1,2</sup>, Nai Yun Chang <sup>2</sup>, Chuan Li <sup>2,3,\*</sup> , Vincent Chan <sup>4,\*</sup>, Jang Hsin Hsieh <sup>5,\*</sup>, Ya-Hui Tsai <sup>6</sup>   
and Tingchao Lin <sup>7,8</sup>

<sup>1</sup> Division of Cardiovascular Surgery, Department of Surgery, Taoyuan Armed Forces General Hospital, Taoyuan 32551, Taiwan; eustonpluto@gmail.com

<sup>2</sup> Department of Biomedical Engineering, National Yang Ming Chiao Tung University, Taipei 11221, Taiwan; abcluluchang@gmail.com

<sup>3</sup> Department of Mechanical Engineering, National Central University, Jhongli, Taoyuan 32001, Taiwan

<sup>4</sup> Department of Biomedical Engineering, College of Engineering, Khalifa University, Abu Dhabi P.O. Box 127788, United Arab Emirates

<sup>5</sup> Center for Plasma and Thin Film Technologies, Ming Chi University of Technology, New Taipei City 24301, Taiwan

<sup>6</sup> Department of Surgery, Far Eastern Memorial Hospital, Banqiao, New Taipei City 22060, Taiwan; yahuitsi@gmail.com

<sup>7</sup> Division of Cardiovascular Surgery, Heart Center, Cheng Hsin General Hospital, Taipei 11246, Taiwan; tingchaolin@gmail.com

<sup>8</sup> Institute of Emergency and Critical Care Medicine, National Yang Ming Chiao Tung University, Taipei 11221, Taiwan

\* Correspondence: cli10@nycu.edu.tw (C.L.); vincent.chan@ku.ac.ae (V.C.); jhhsieh2@gmail.com (J.H.H.); Tel.: +886-2-2826-7397 (C.L.)



**Citation:** Chi, H.Y.; Chang, N.Y.; Li, C.; Chan, V.; Hsieh, J.H.; Tsai, Y.-H.; Lin, T. Fabrication of Gelatin Nanofibers by Electrospinning—Mixture of Gelatin and Polyvinyl Alcohol. *Polymers* **2022**, *14*, 2610. <https://doi.org/10.3390/polym14132610>

Academic Editor: Khalil Ab-delrazek Khalil

Received: 30 May 2022

Accepted: 20 June 2022

Published: 27 June 2022

**Publisher's Note:** MDPI stays neutral with regard to jurisdictional claims in published maps and institutional affiliations.



**Copyright:** © 2022 by the authors. Licensee MDPI, Basel, Switzerland. This article is an open access article distributed under the terms and conditions of the Creative Commons Attribution (CC BY) license (<https://creativecommons.org/licenses/by/4.0/>).

**Abstract:** Gelatin, one of the most abundant, naturally derived biomacromolecules from collagen, is widely applicable in food additives, cosmetic ingredients, drug formulation, and wound dressing based on their non-toxicity and biodegradability. In parallel, polyvinyl alcohol (PVA), a synthetic polymer, has been commonly applied as a thickening agent for coating processes in aqueous systems and a major component in healthcare products for cartilage replacements, eye lubrication, and contact lenses. In this study, a new type of mixed hydrogel nanofiber was fabricated from gelatin and polyvinyl alcohol by electrospinning under a feasible range of polymer compositions. To determine the optimal composition of gelatin and polyvinyl alcohol in nanofiber fabrication, several key physicochemical properties of mixed polymer solutions such as viscosity, surface tension, pH, and electrical conductance were thoroughly characterized by a viscometer, surface tensiometer, water analyzer, and carbon electron probe. Moreover, the molecular structures of polymeric chains within mixed hydrogel nanofibers were investigated with Fourier-transform infrared spectroscopy. The morphologies and surface elemental compositions of the mixed hydrogel nanofibers were examined by the scanning electron microscope and energy-dispersive X-ray spectroscopy, respectively. The measurement of water contact angles was performed for measuring the hydrophilicity of nanofiber surfaces. Most importantly, the potential cytotoxicity of the electrospun nanofibers was evaluated by the in vitro culture of 3T3 fibroblasts. Through our extensive study, it was found that a PVA-rich solution (a volumetric ratio of gelatin/polyvinyl alcohol < 1) would be superior for the efficient production of mixed hydrogel nanofibers by electrospinning techniques. This result is due to the appropriate balance between the higher viscosity ( $\sim 420\text{--}4300\ 10^{-2}$  poise) and slightly lower surface tension ( $\sim 35.12\text{--}32.68\ \text{mN/m}^2$ ) of the mixed polymer solution. The regression on the viscosity data also found a good fit by the Lederer–Rouquier’s model for a binary mixture. For the hydrophilicity of nanofibers, the numerical analysis estimates that the value of interfacial energy for the water contact on nanofibers is around  $\sim -0.028$  to  $\sim -0.059\ \text{J/m}^2$ .

**Keywords:** gelatin; polyvinyl alcohol; electrospinning; spin coating; Fourier-transform infrared spectrometer; water contact angle

## 1. Introduction

Among recently developed biomedical materials, polymeric electrospun nanofibers have emerged as one of the most promising platforms for building multifunctional scaffolds in wound treatment. In general, modern wound dressings must embrace several key functions including the reduction of bleeding, acceleration of blood coagulation, protection of wounded tissues from infection, absorption of exudate, prevention of maceration, stimulation of tissue regeneration, and alleviation of pain with analgesic or antibacterial medications [1–5]. To date, innovative wound dressings rendered with superior bioactivities and engineered precisions can be fabricated into various formats such as porous scaffolds or implants with the use of additive manufacturing for the treatments of various diseases [6–8]. In particular, the multicomponent electrospun nanofibers composed of polymeric complex coacervates are superbly fit for the development of novel wound dressing based on their large surface-area-to-volume ratio, high water retention, and unmatched versatility in material selections.

The biomedical applications of hydrogel nanofibers have gone beyond wound dressing. With assorted compositions, ingenious designs, and economical fabrications, hydrogel nanofibers have been used for drug delivery, tissue engineering, and prosthetic products depending on material properties and functions. For example, poly(ethylene-co-vinyl alcohol) (EVOH) in a nanofiber mesh is capable of selectively adsorbing uremic toxins such as creatinine for potential filtration in kidney dialysis [9]. Poly(ethylene oxide) (PEO) and PVA nanofibers, either in the form of blend or core-shell, can encapsulate drugs with a controlled release feature [10]. The superabsorbent textiles of polyvinylpyrrolidone (PVP) and polyacrylic acid (PAA) can be made for gauze sponges [11]. Slowly degradable polyphenols can be coated on orthopedic implants to promote bone regeneration. When added to nanofiber scaffolds, polyphenols even showed some antioxidant effects [12]. Silk fibroin nanofibers, a complicated natural hydrogel, are a respectable constituent in artificial skin, considering their exceptional biocompatibility [13].

The two most critical requirements of advanced wound dressing are biocompatibility and nontoxicity, regardless of the site of implementation, and they are fulfilled by various types of electrospun nanofibers. Specifically, polymeric hydrogels derived from naturally occurring biomacromolecules from animals or plants have demonstrated exceptional biocompatibility and ideal biodegradability under a range of *in vivo* conditions [14–17]. Among various natural hydrogels, gelatin is perhaps the most abundant of proteins derived from collagen commonly found in the connective tissues of animals. Gelatin is generally produced from the irreversible hydrolysis and denaturation of collagen boiling with the use of acids (type A) or alkalis (type B) [18–22]. The exact compositions of gelatin in terms of amino acid sequences vary based on the source and extraction methods. In general, gelatin isolated from various types of animal tissues is translucent under visualization at room temperature and rich in glycine, proline, hydroxyproline, alanine, etc. [23–27]. After gelatin synthesis, various purification steps including filtration, evaporation, refining, recovery, drying, or grinding are applied to form the final products [18–22]. Gelatin is also used as an additive in food, cosmetics, or medicine [28–32].

Alternatively, hydrogels composed of synthetic polymers such as poly(vinyl alcohol) (PVA,  $[\text{CH}_2\text{CH}(\text{OH})]_n$ ) emerge as a simple and low-cost thickening agent that has been extensively applied in the manufacturing of several biomedical products such as contact lenses, stents, and cartilage implants [33–37]. Similar to gelatin, PVA is a water-soluble and biocompatible polymer, serving as a good adhesive for bonding insulators such as wood and paper. Moreover, PVA is produced in the form of colorless and odorless powders, which readily dissolve in water to form a viscous liquid [37]. Interestingly, the gelation of a PVA solution enables the combination of PVA with other molecular constituents such as borate (boron–oxygen compounds) to fabricate novel hydrogel with enhanced mechanical properties for various biomedical applications under physiological conditions [38].

Although the potential fabrication of gelatin into nanofibers sounds attractive for advanced biomedical applications, a pure gelatin solution is not a feasible choice for direct

electrospinning. For instance, the gelation and melting temperatures of gelatin derived from goats are found to be around 25.14–25.23 and 34.09–34.18 °C, respectively. The thermal properties mentioned above lead to the rapid solidification of the gelatin solution into a solid at the operation temperature (23 °C) of conventional electrospinning [39]. At the same time, the low surface charge density of gelatin prohibits effective nanofiber formation during electrospinning. Most importantly, the highly sensitive, temperature-dependent viscosity of the gelatin solution imposes a significant challenge in the preparation of practically feasible gelatin solutions for electrospinning or spin coating. The shared physicochemical properties between gelatin and PVA as mentioned above have attracted the attention of some researchers for fabricating novel gelatin/PVA composite scaffolds for emerging applications in tissue engineering [10,11,33–37]. To date, the formation of electrospun gelatin/PVA hydrogel nanofibers has not been systematically studied against different experimental conditions. Such an approach of blending between gelatin and PVA will potentially stabilize the nanofiber formation from electrospinning.

It has been shown that acetic acid at sufficiently high concentrations can reduce the molecular weight of gelatin through hydrolysis of a fraction of the peptide bonds along the polymeric backbone of gelatin [19–22]. Specifically, the hydrolysis effectively prevents the rapid solidification of the gelatin solution at room temperature and enables the effective mixing of gelatin with PVA in the liquid phase. Therefore, the preparation of a gelatin/PVA polymer solution that is applicable for both spin coating and electrospinning should be achievable by applying a certain concentration of acetic acids during the mixing of the two polymers.

In this study, we fabricated gelatin/PVA nanofibers by electrospinning on top of a hydrogel film of identical compositions produced by spin coating. The structure, morphology, and compositions of the gelatin/PVA nanofibers were systematically examined against a range of physicochemical properties of polymer solution mixtures. In particular, the viscosity, surface tension, electrical conductance, and pH of gelatin/PVA polymer solutions used in the fabrication of hydrogel nanofibers and films were examined by a viscometer, surface tensiometer, digital carbon electrode, and digital electrochemical probe, respectively. Afterward, a scanning electron microscope (SEM) was applied to probe the surface morphology, while a Fourier-transform infrared spectrometer (FTIR) was applied to probe the chemical structures, and water contact angle measurement was used to evaluate the hydrophilicity of gelatin/PVA nanofibers prepared from different polymer solution mixtures. To test the cytotoxicity of gelatin/PVA nanofibrous film, MTT assays of cultured 3T3 fibroblasts for determining the live/dead cell ratio were performed. Overall, the interrelation between polymer solution properties, hydrogel nanofiber structures, and cellular responses was elucidated herein for enabling the future development of highly engineered gelatin/PVA nanofibers in specific applications.

## 2. Experimental Procedure

The design of the gelatin/PVA nanofiber-film pack is depicted in Figure 1 where both the layer film and nanofibers are made of mixed gelatin (12 wt. % in DI water) with acetic acids (10 vol. % in DI water), and/or PVA (12 wt. % in DI water) is formed by spin coating and electrospinning, respectively. The main purpose of adding acetic acids to gelatin is to prevent the solidification of gelatin at room temperature. There is no such need for pure PVA solution since the pure PVA is already in the liquid state at room temperature. For all testing and material characterizations, we place the whole pack on a glass substrate for easy handling and observations of cell culture.

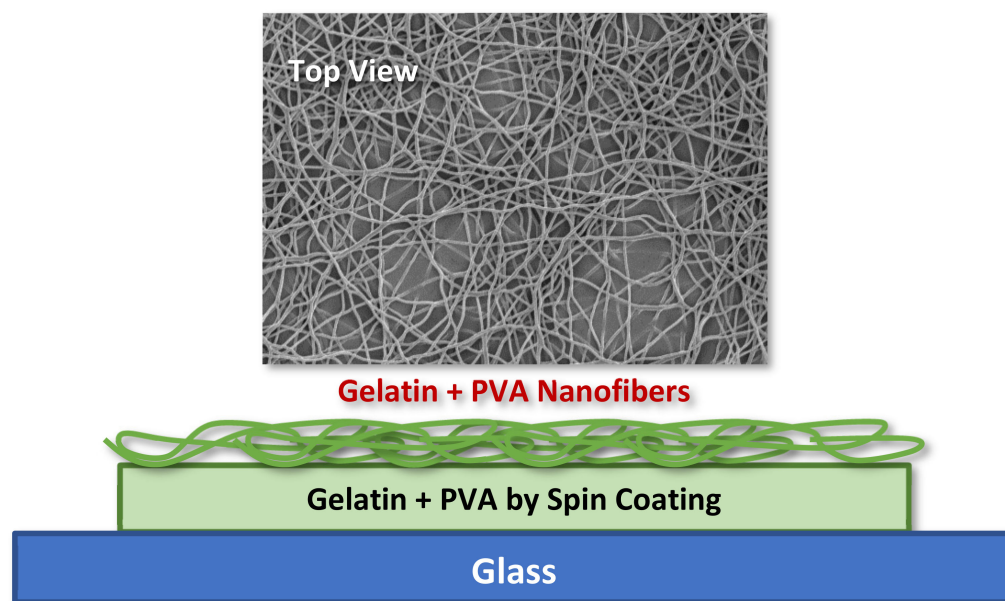


**Figure 1.** Morphology of electrospun gelatin/PVA mixed nanofibers on top of a film made of identical material.

### 2.1. Substrate and Materials

Corning glass (Corning 1737) was cut into  $10 \times 10 \text{ mm}^2$  pieces by tungsten cutter and then ultrasonically cleaned in KOH (85%), acetone (99.9%), DI water, and alcohol (90%) alternatively. Each cleaning took around 10 min. After clean-up, the cut glass was blown dry by nitrogen. For the cell culture, all deposited film samples were radiated by UV light for at least 15 min and then placed in a 24-well dish for all biological tests.

Purchased gelatin (2013-0311-076, major amino acids: AGPRGEOGPG,  $\sim 20.6$  cps, Emperor Chemical Co., Ltd., Taipei, Taiwan) in the form of white to light yellow powders was dissolved in DI water and acetic acid (2013-0208-022, 99.5%, Emperor Chemical Co., Ltd., Taipei, Taiwan) then continuously stirred for 1–2 h  $\sim 70^\circ\text{C}$  before being used for spin coating or electrospinning. The concentration of gelatin and acetic acids is listed in Tables 1 and 2.

**Table 1.** Parameters for spin coating of gelatin/PVA mixed layer film.

Process Parameters for Gelatin/PVA Films by Spin Coating	
Speed (rpm)	3000
Operational temperature ( $^\circ\text{C}$ )	Room temperature
Deposition time (second)	60
Gelatin concentration in DI water (wt. %)	12
PVA concentration in DI water (wt. %)	12
Acetic acid concentration in DI water (vol. %)	10 mL/100 mL (10%)
Mixture of polymeric solution volume ratio (vol. %)	8:2, 6:4, 5:5, 4:6, 2:8, 0:10 in total 10 mL

**Table 2.** Parameters for electrospinning gelatin/PVA mixed nanofibers.

Process Parameters for Gelatin/PVA Nanofibers by Electrospinning	
Voltage (kV)	12–12.5
Syringe pumping speed ( $\mu\text{L}/\text{min}$ )	$1 \times 10^{-2}$
Syringe outer/inner diameter (mm)	$5.0 \times 10^{-1}/2.6 \times 10^{-1}$
Operational temperature ( $^\circ\text{C}$ )	Room temperature
Working distance (cm)	12
Deposition time (sec)	>60

PVA ( $\sim 120,000$ – $132,000 \text{ g/mol}$ ,  $\sim 36$ – $42$  cps, 2013-0401-084, Emperor Chemical Co., Ltd., Taipei, Taiwan) in white powders was dissolved in DI water and then continuously stirred

for 1–2 h at room temperature before being used for spin coating or electrospinning. The concentration of PVA is also listed in Tables 1 and 2.

In this study, we tested gelatin and PVA solutions mixed at different volumetric ratios prepared for films by spin coating, and nanofibers by electrospinning. This information is crucial for the production of such nanofibers at large scales.

## 2.2. Spin Coating

The gelatin/PVA layer film is formed by spin coating (SWIENCO SP-02, Power Assist Instrument Scientific Corp. Taoyuan, Taiwan) using mixtures of gelatin/PVA solution. The optimized rotation speed was set to 3000 rpm from different films. All coating processes took 1 min to allow the solution to spread large enough to cover the glass substrate. After coating, we let the sample rest calmly for less than 30 min before electrically spinning the nanofibers on top.

## 2.3. Electrospinning

The electrospinning of gelatin/PVA was carried by a commercial system (FES-COE, Falco, Taiwan) where the system consists of a syringe pump, a power supply, and a horizontally movable platform (collector) to carry the substrate.

The dissolved gelatin/PVA solution was first drawn into a syringe tube before ejecting onto a substrate. Parameters for the operation of the electrospinning system are listed in Tables 1 and 2. Note that particularly in the electrospinning, the distances between the needle and substrate and voltage are all adjusted by trial and error in a preliminary study to have an optimal result of deposited gelatin/PVA with uniform thickness. We skip details for the conciseness of this report. Moreover, the formation of nanofibers is mostly unaffected by the compositions of gelatin/PVA using the current equipment. The dimension (diameter) of nanofibers is controlled by both voltage and syringe pumping speed. In general, the higher the applied voltage or pumping speed, the thinner the fibers that are produced. However, excessively high voltage can induce arching between the substrate and needle, which leads to the breakup of a jet into droplets. Parameters in Tables 1 and 2 were chosen by many rounds of trials to assure the successive reproduction of gelatin/PVA nanofibers.

## 2.4. Characterization

### 2.4.1. Viscosity of Polymer Solution

The viscosity of gelatin and PVA mixed solution is measured by a viscometer (DV2T, Brookfield AMETEK, Middleborough, MA, USA). The measurement was carried out at room temperature with a spindle (SC4-27D). The rotational velocity is set at 20 rpm for generating enough torque. It is suggested by the manufacturer to have at least 10% of the maximum torque to obtain accurate measures for viscosity. The measured viscosity is automatically recorded by the system every 15 s. An accurate measure typically takes about 2–5 min until the fluid flow reaches a steady state. Each sample solution was repeatedly measured 3 times, and the average was calculated.

### 2.4.2. Electrical Conductivity and pH Value of Polymer Solution

The electrical conductance and pH of gelatin/PVA solutions were measured by a multiple-purpose water analyzer (WA-2017SD-Water Analysis, Lutron, Taiwan). For the pH measurement, an electrochemical probe (PE-03) is connected to a multiple-purpose datalogger for detection, whereas for the measurement of electrical conductance, a carbon electrode (CDPB-03) is instead used with a connection to the same datalogger.

For better accuracy, three measurements were taken for both electrical conductance and pH value in each sample solution to have averaged values.

### 2.4.3. Surface Tension of Polymer Solution

The surface tension of gelatin and PVA mixed solutions is measured by a digital surface tensiometer (BZY-IV, Hengping Instrument Ltd., Shanghai, China). The measurement follows the Wilhelmy plate method. A rectangular iridium–platinum plate of dimensions 23.8 mm (w) × 10 mm (h) × 0.43 cm (t) is first dipped into the liquid and then gradually pulled back by a thin wire to its original position before dipping. The whole process is precisely controlled by a height-adjustable table that carries a glass beaker of liquid while a stationary fixture hangs the plate still. During the pulling, liquid lamella snaps on the plate, and the force balance between the weight of lamella and the liquid/plate interfacial tension leads to the Wilhelmy equation:

$$\gamma_{LP} = \frac{F}{l_{wet} \cos \theta} \quad (1)$$

where  $\gamma_{LP}$  is interfacial tension (energy) between the liquid and plate,  $F$  is the measured hanging force through the wire,  $l_{wet}$  is the wetted perimeter ( $2 \times (\text{width} + \text{thickness})$ ), and  $\theta$  is the contact angle between the liquid and the plate. In practice, the difficulty of measuring contact angle is either replaced by values from the literature if the liquid is well known or assuming complete wetting ( $\theta = 0$ ) instead. In this study, complete wetting is assumed because both dipping and pulling are slow (2–3 min), and we added a period of waiting after submerging.

### 2.4.4. Surface Morphology of Layer Film and Nanofibers

The morphology of electrospun gelatin/PVA fibers was imaged and estimated by scanning electron microscope (SEM, S-3400N, Hitachi, Japan). For SEM, the voltage of the accelerated electron beam is set at 15 kV, the working distance is 10,300  $\mu\text{m}$ , the emission current is 88,000 nA, and the magnification is chosen to be 3000 for the best resolution.

### 2.4.5. Chemical Element Analysis of Layer Film and Nanofibers

The average elemental compositions of electrospun gelatin/PVA fibers under SEM inspection were measured by energy-dispersive X-ray spectroscopy (EDS, EDS, Bruker Nano, XFlash Detector 5010, German) using a 15 kV electron beam; the counting per second (cps) is between 2000–3000, and scanning area is around  $1500 \times 1125$  pixels. The magnification was chosen to be 3000 too. The selected chemical elements subjected to analysis are C, O, and N from the radiation of the  $K\alpha$  series.

### 2.4.6. Molecular Structure of Layer Film and Nanofibers

To determine the vibrational modes of molecular bonding in the deposited gelatin/PVA layer films, Fourier-transform infrared spectrometer (FTIR, V-770, Jasco USA, equipped with single monochromators and dual detectors) was used to detect the infrared absorption in the range of 650–4000  $\text{cm}^{-1}$  with a resolution of 1  $\text{cm}^{-1}$  in the reflection mode. An uncoated glass substrate was first detected, and its spectrum is used as a reference to differentiate the spectrum from coated samples. During measurement, the detector is in line with the sample at its backside. The spectrum was numerically analyzed by Fityk 0.9.8 using Gaussian fitting to identify possible absorption peaks for different vibrational modes of various chemical bonds. Major absorption peaks of optical emission relevant to gelatin/PVA films are listed in Table A1 in Appendix B for later discussion [40–50].

### 2.4.7. Contact Angle of Layer Film and Nanofibers

The contact angles of electrospun gelatin/PVA fiber films were measured from the image of water droplets (1 mL) on samples and shot by a CCD camera (Watec, WAT-902B, Watec Corp., Tsuruoka, Yamagata, Japan). Images were first uploaded to the “Online Protractor” ([https://www.ginifab.com/feeds/angle\\_measurement/](https://www.ginifab.com/feeds/angle_measurement/), accessed on 1 March 2022), and then the contact angle of drops on substrates could be measured.

### 3. In Vitro Cell Culture

#### 3.1. Cell Preparation

3T3 fibroblasts purchased from (ATCC, CCL-92<sup>TM</sup>, 3T3-Swiss albino, Research Center, Hsinchu, Taiwan) are ready for the experiment. The cells, stored in tubes and kept in a  $-20\text{ }^{\circ}\text{C}$  freezer, were first bathed and shaken in  $37\text{ }^{\circ}\text{C}$  water for about 30 min. After completely warming up, cells are pipetted into a culture medium (Dulbecco's Modified Eagle Medium/High Glucose powder, Gibco<sup>®</sup>, Thermo Fisher Scientific, Waltham, MA, USA) inside a 6 cm diameter Petri dish. Using our own established protocol, 3T3 fibroblasts were cultured in an incubator (2424IR, ShelLab-Sheldon Manufacturing Inc., Cornelius, OR, USA) under a controlled environment, i.e.,  $37\text{ }^{\circ}\text{C}$ , 5%  $\text{CO}_2$ , and 95% relative humidity, for 2 to 3 days before they were trypsinized and pipetted into tubes. This suspension was then centrifuged for 5 min at 1500 rpm. After centrifugation, cells in the sediment mixed with culture medium were pipetted out and dropped into a 6- or 24-well plate for further tests.

Note that for the cell culture, all fiber film samples were radiated by UV light for at least 30 min and then placed in a 24-well dish before biological tests.

#### 3.2. Cell Viability Test

To access the cell viability of 3T3 by in vitro culture, the culture processes were explained as follows. We first immersed electrospun gelatin/PVA samples in  $500\text{ }\mu\text{L}$  of Dulbecco's Modified Eagle Medium (DMEM) inside a 24-well plate. Then, 3T3 fibroblasts (25,000 cells/well) were directly seeded on each well. After 48 h, images of seeded cells were taken under an optical microscope ( $50\times$ ). After imaging, the DMEM was abstracted and proceeded to the MTT assay.

Another seeding process is to immerse fiber film samples in the 24-well plate and seed the 3T3 fibroblasts (25,000 cells/well) directly on the samples. After 48 h, optical images of seeded cells on samples were taken, and the DMEM was abstracted for the MTT assay.

#### 3.3. MTT Assay

The viability of cells is evaluated by MTT assay. MTT is a yellowish and water-soluble tetrazolium salt (3-[4,5-dimethylthiazol-2-yl]-2,5-diphenyltetrazolium-bromide). If there is nicotinamide adenine dinucleotide (generated by active metabolism in cells, its oxidized and reduced forms shortened as  $\text{NAD}^+$  and  $\text{NADH}$ , respectively) present in the solution, MTT can then be reduced to an insoluble purple formazan. This insoluble formazan shall deposit on the cell surface and can be dissolved in isopropanol or other organic solvents. The dissolved solution has signature optical absorbing peaks at 550 and 650 nm identifiable by a spectrometer (Epoch 2, Microplate Spectrophotometer, BioTek Instruments Inc. Santa Clara, CA, USA), the intensities of which are proportional to the concentration of formazan. As MTT is found in all living cells, its concentration can be used as a marker to quantify the number of viable cells. The intensity of absorption peaks is usually expressed as optical density (OD), which is defined as

$$\text{OD} = \log_{10} \left( \frac{\text{incident light intensity}}{\text{transmitted light intensity}} \right) \quad (2)$$

The steps of the MTT assay are described as follows. The abstracted DMEM was mixed with  $200\text{ }\mu\text{L}$  MTT (0.5 mg/mL in 1X PBS) and pipetted into a 24-well plate. The plate was kept in the incubator for 2–4 h and then examined by an optical microscope. If crystalline formazans (filaments) were found in cells, another  $600\text{ }\mu\text{L}$  dimethyl sulfoxide (DMSO,  $(\text{CH}_3)_2\text{SO}$ ) was then added to each well to dissolve formazans. After around 5 min,  $200\text{ }\mu\text{L}$  of DMSO-added culture media was abstracted from each well and distributed into a 96-well plate. This plate was sent to the spectrometer for measuring the optical absorption by liquid at 550 nm and 650 nm.

## 4. Results

### 4.1. Characterizations for Polymer Solution

#### 4.1.1. Viscosity

Whether mutually miscible gelatin and PVA solutions have an impact on the polymeric solution prepared for electrospinning remains to be investigated. Figure 2 demonstrates the variation of viscosity according to different gelatin/PVA volumetric concentrations. The variation seems to follow an exponential function by numerical fitting with a coefficient of determination of  $\sim 0.9723$ .

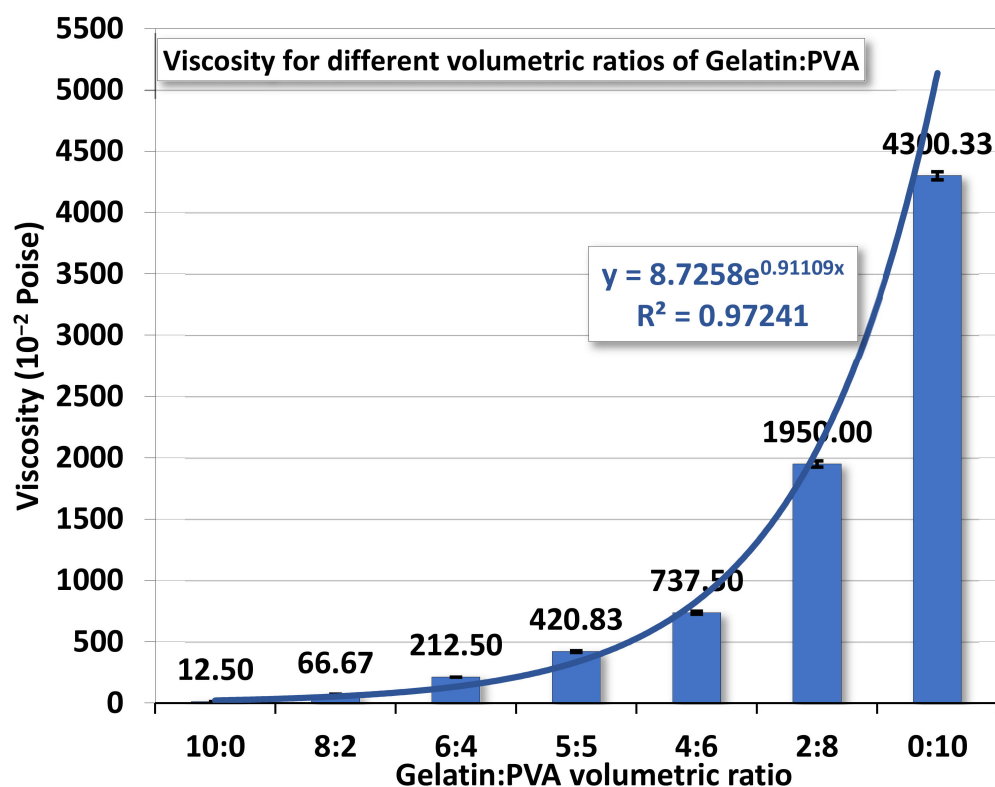


Figure 2. The averaged viscosity of gelatin/PVA mixed solution.

The variation of viscosity is much like a continuous function without a first- or second-order phase change. In other words, the mutually miscible gelatin and PVA solution should not involve chemical reactions. For the pure gelatin solution, the low viscosity, 12.5 centipoises, reflects its high solubility in DI water while the pure PVA (12 wt. %) having a viscosity reaching 4300.33 centipoises implies a much higher resistance to water dissolution. This phenomenon is largely attributed to the difference in the molecular structures of the two polymers. The gelatin has a long chain of amino acids vulnerable to hydrogen bonding by water molecules, whereas the smaller and more compact secondary alcohol structure ( $\text{—CH}_2\text{—OH}$ ) in PVA is better for resisting such water bonding [51].

#### 4.1.2. Electrical Conductance

Figure 3 shows the electrical conductance of a polymer solution against the change of gelatin/PVA volumetric or concentration ratio in the polymer solution mixture. The result showed that the electrical conductivity for the gelatin/PVA solution mixture was lowered against the increase in the relative amount of PVA. For the pure PVA solution (12 wt. %), the electrical conductivity was lowest at  $1.5 \times 10^{-4}$  S in the absence of acetic acid among all samples used herein. This was because PVA has a low degree of ionization, even at lower pH [52]. Interestingly, higher electrical conductivity was detected in all gelatin/PVA mixtures compared to that of pure PVA. The result was mainly promoted by the presence of acetic acids used for gelatin dissolution (for all gelatin-containing mixtures), leading to

higher ionic strength in DI water [19–22]. So, even for the solution of gelatin/PVA ratio at 2:8, the solution conductivity, measured to be around  $5.9 \times 10^{-4}$  S, is still about four times higher than that of the pure PVA solution.

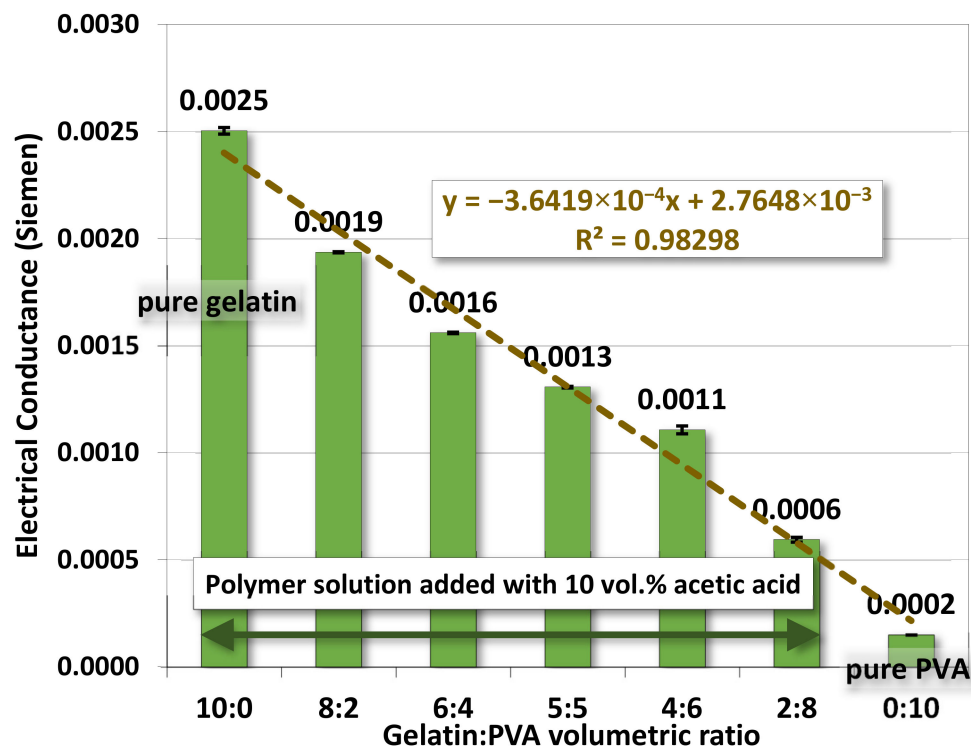


Figure 3. The average electrical conductance of gelatin/PVA mixed solutions.

The variation of electrical conductivity for gelatin/PVA mixed solutions is numerically fitted well by a linear function with the coefficient of determination  $R^2 = 0.975$ . These fitting results provide a guideline for the preparation of polymer solutions in successive studies.

#### 4.1.3. pH Value

The variation of pH values for gelatin/PVA mixed solutions, shown in Figure 4, is influenced by the adding acetic acids. For various gelatin/PVA mixed solutions, the pH values increase as the gelatin content is reduced. However, the change in pH value is very minor (3.30 for gelatin/PVA = 10:0 to 3.59 for gelatin/PVA = 2:8) because the whole solution is primarily a mixture of nothing but weak acids - amino acids, acetic acids, and PVA (the pH value of pure PVA without acetic acids is around 5.5). Note that most acetic acids will evaporate out when layer films or nanofibers start to form through solidification in the process of spin coating and electrospinning.

Variations of the pH values are also numerically fitted against the change of gelatin/PVA volume ratio. Similar to the case of electrical conductivity, a linear function is found with a high coefficient of determination  $R^2 = 0.966$ .

#### 4.1.4. Surface Tension

The surface tension for gelatin/PVA mixed solutions is shown in Figure 5. Values of surface tension decrease as the PVA concentration increases. A linear polynomial function is found to fit measurements with  $R^2 = 0.982$ . Pure PVA has a higher viscosity, but its surface tension is nevertheless lower than all other mixed solutions. These two opposites combined can be very helpful in the formation of nanofibers by electrospinning, as lower surface tension facilitates the stretching by the electrical field while higher viscosity prevents the disintegration of fibers into droplets (see SEM in the next section).

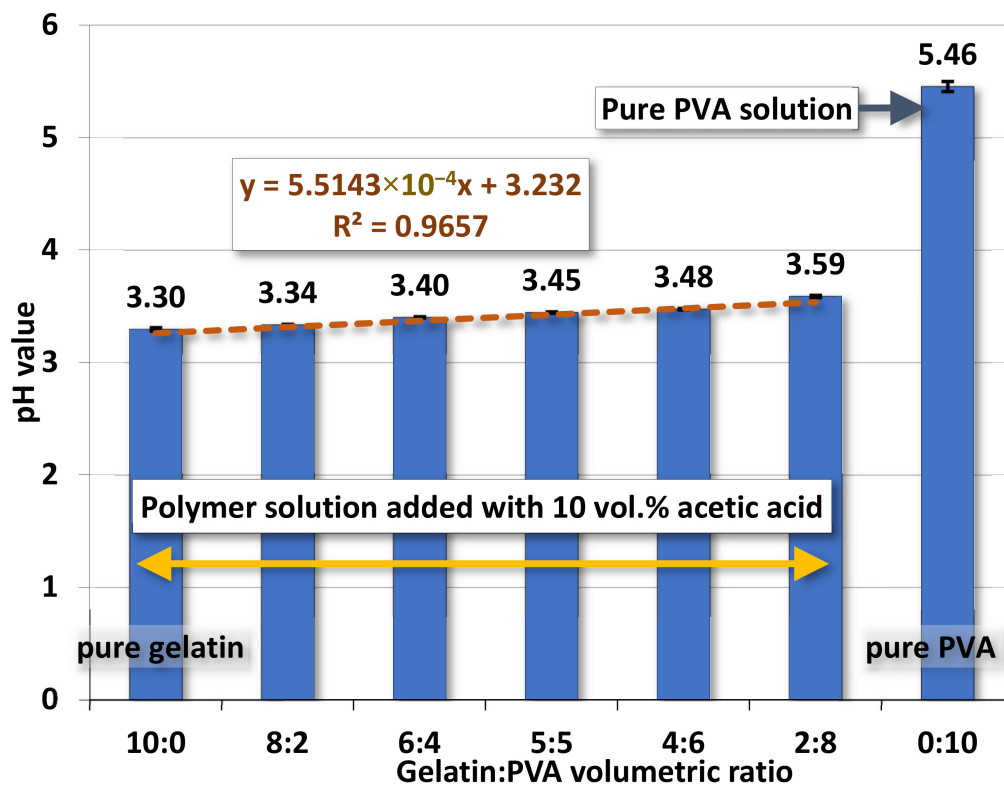


Figure 4. The average pH values of gelatin/PVA mixed solutions.

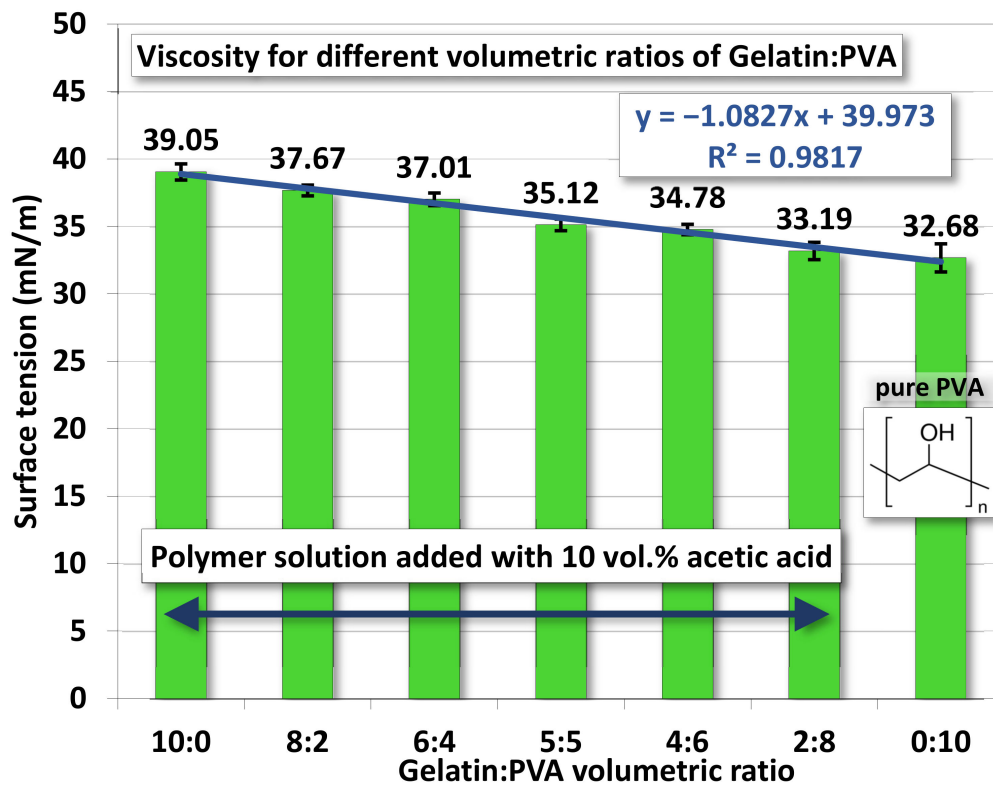
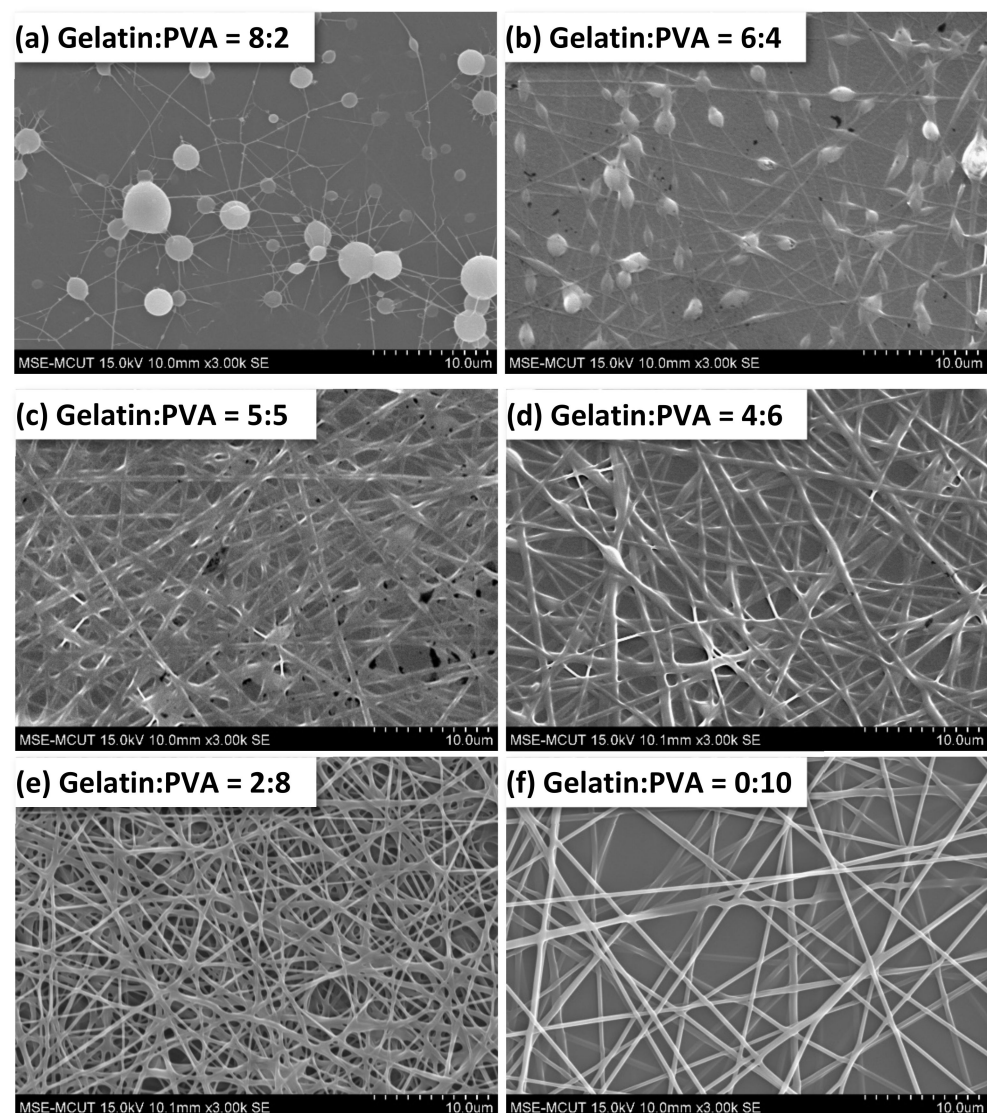


Figure 5. The average surface tension of gelatin/PVA mixed solutions.

## 4.2. Characterizations for Layer Films and Nanofibers

### 4.2.1. Morphology of Nanofibers

The SEM images of gelatin/PVA nanofibers are presented in Figure 6. It shows that no fibers were formed by electrospinning at low PVA concentrations (Figure 6a the volumetric ratio of gelatin/PVA = 8:2). As the content of PVA increases, the nanofibers start to form as shown in Figure 6b (the volumetric ratio of gelatin/PVA changes to 6:4). The mixed gelatin/PVA fibers shown in Figure 6c at a volumetric ratio of 5:5 seem to be mutually miscible; therefore, much thicker fibers are observed. As the PVA concentration becomes a dominant composition, i.e., the volumetric ratio of gelatin to PVA is lower than 5:5, nanofibers become thinner, less overlapping, and tangling (Figure 6d–f). Less overlapping and tangling implies two phenomena: the higher stretching of jets and the easy whipping of nanofibers.



**Figure 6.** Morphology of electrospun gelatin/PVA mixed nanofibers on top of a film.

To quantify the nanofibers' dimension, we randomly selected fibers from each SEM image and measured their diameters. The average diameters of fibers in different samples are shown in Figure 7. The range of average diameters of fibers falls between 287 and 541 nm, but the diameters of pure 50:50 gelatin/PVA fibers are larger than other samples. The formation of larger diameters can be attributed to the thinning of jets and mutually miscible gelatin and PVA solutions, as observed in the SEM images.

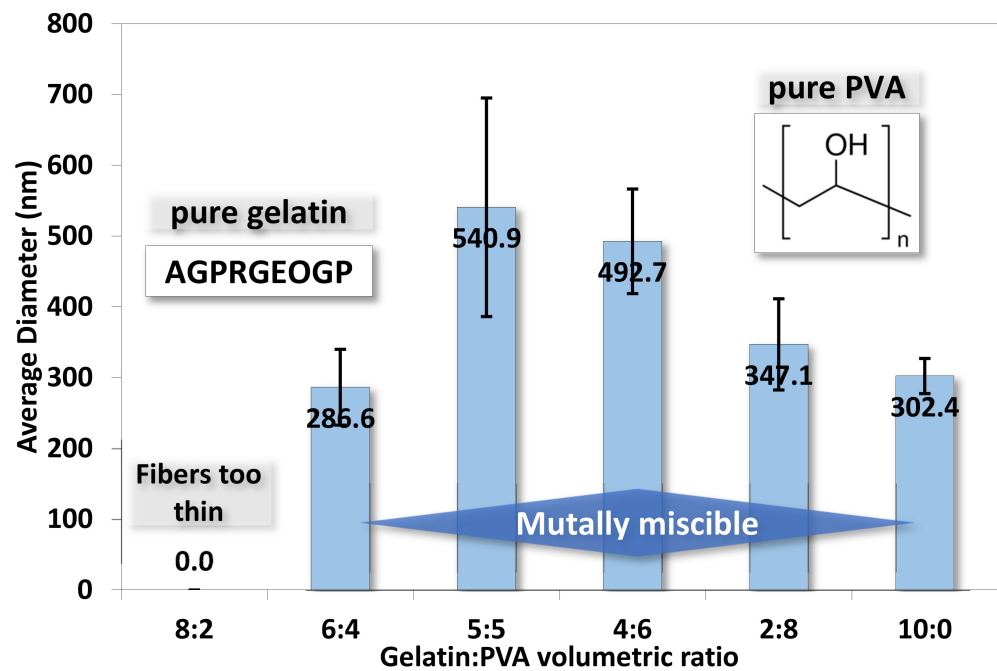


Figure 7. The averaged diameters for electrospun gelatin/PVA mixed nanofibers. (The symbols for amino acids are A: alanine, G: glycine, P: proline, R: arginine, E: glutamate, and O: hydroxyproline).

4.2.2. EDS

The chemical element analysis on the surface of gelatin/PVA fiber films is shown in Figure 8 where three elements, carbon, oxygen, and nitrogen, are identified. Note that only a trace of 0.97 at. % is found in pure PVA because no nitrogen exists in PVA. The content of nitrogen in gelatin/PVA fiber films also varies positively according to the increase of gelatin.

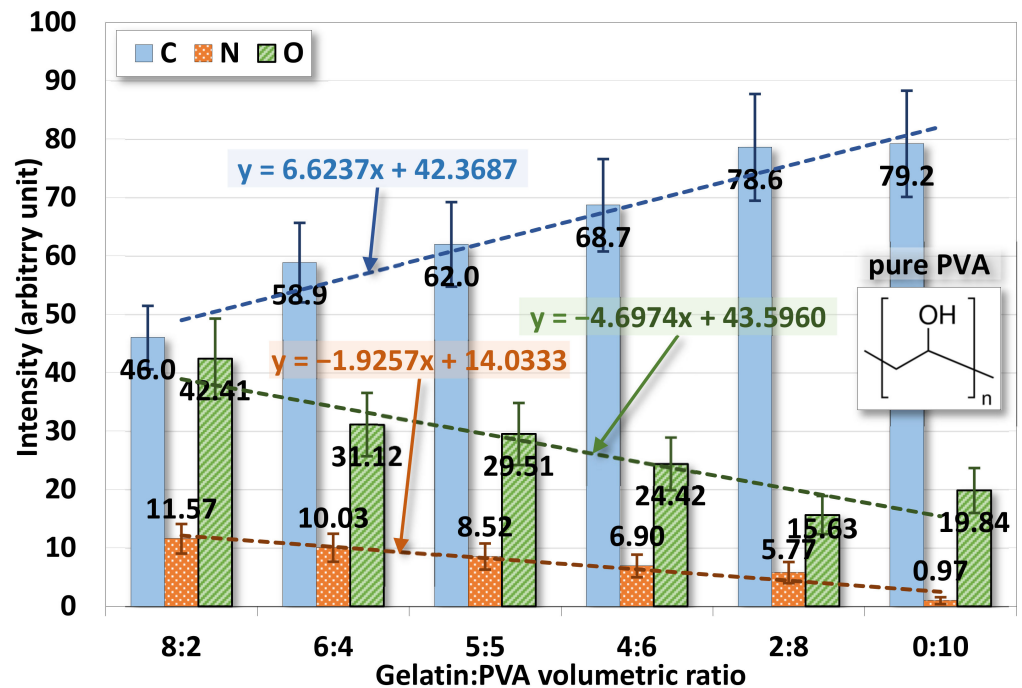
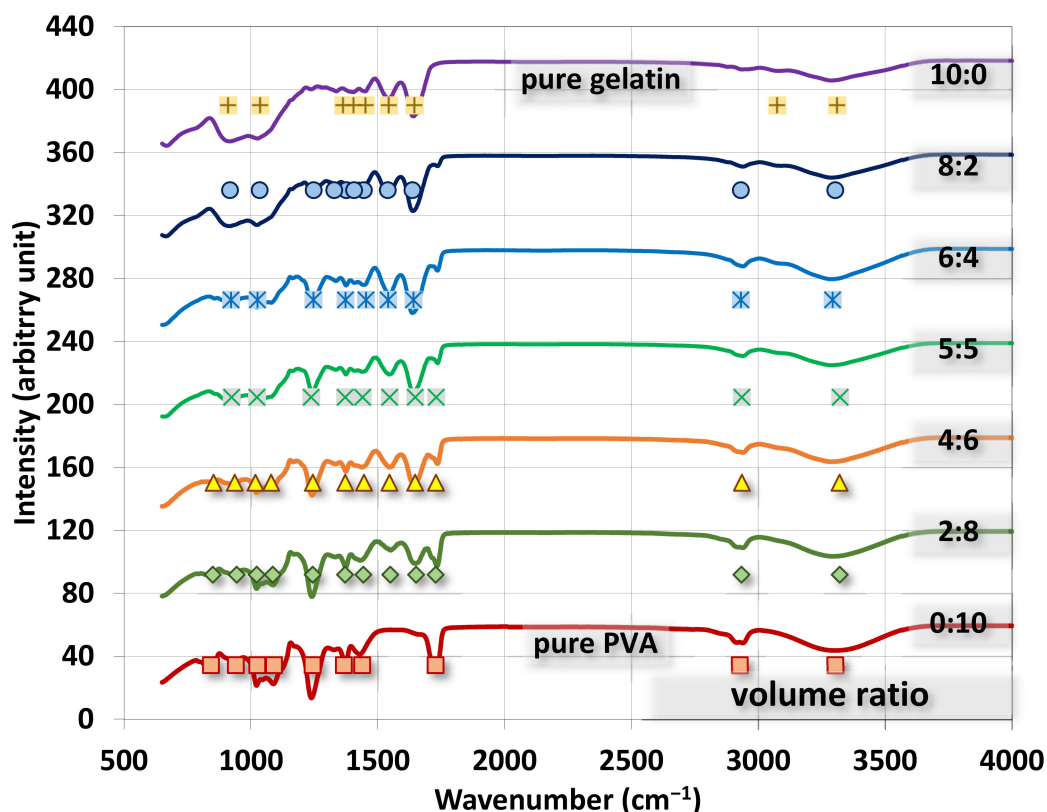


Figure 8. Variations of surface chemical elements from the EDS of electrospun gelatin/PVA mixed nanofibers.

EDS confirms that the chemical compositions of deposited fiber films are directly derived from the polymer solutions prepared for the electrospinning and spin coating. The mixing of gelatin and PVA in DI water is only physical but not chemical.

#### 4.2.3. FTIR

The FTIR spectra for gelatin/PVA fiber films are shown in Figure 9 where all spectra are presented in the range of 650–4000  $\text{cm}^{-1}$  with marks for absorption peaks by Gaussian fitting. We also present spectra for pure gelatin alongside the mixed polymers for benchmark comparison.



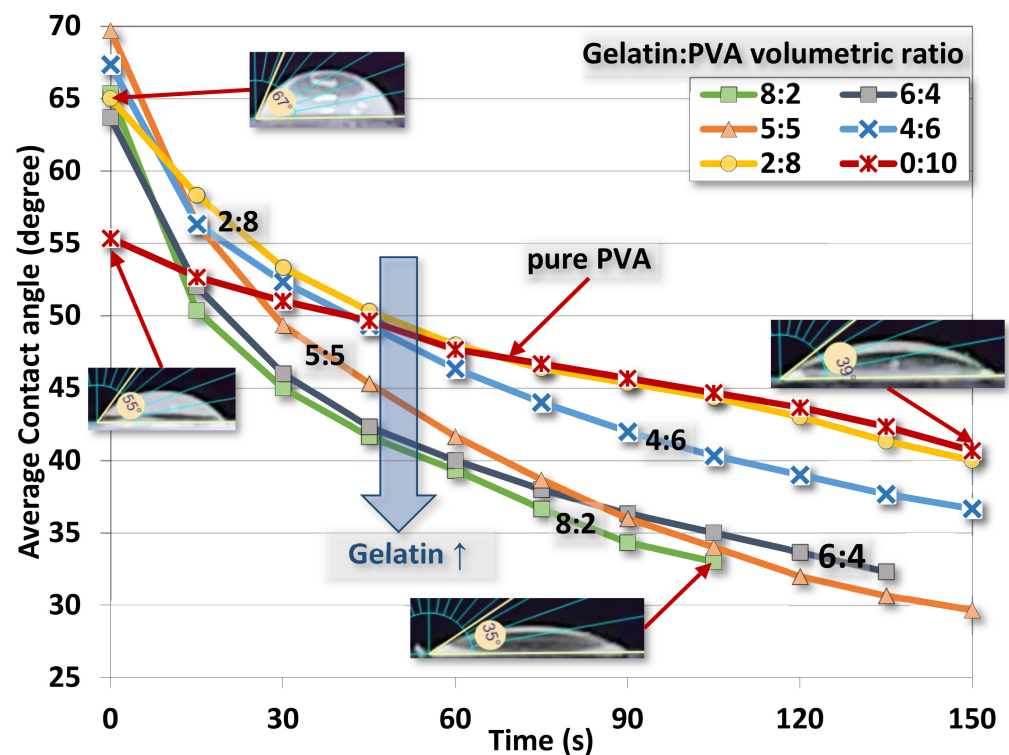
**Figure 9.** FTIR spectra for electrospun gelatin/PVA nanofiber films with different volumetric mixing ratios.

Major FTIR peaks by Gaussian fitting for PVA are found to be a C-O stretch at  $\sim 1243.3 \text{ cm}^{-1}$ , C=O at  $\sim 1728.3 \text{ cm}^{-1}$ , O-C-O in ester groups at  $\sim 1090.9 \text{ cm}^{-1}$ , C-O stretch in acetyl groups at  $\sim 1025.5 \text{ cm}^{-1}$ , O-H stretch at  $\sim 3304.1 \text{ cm}^{-1}$ ,  $\text{CH}_3$  bending at  $\sim 1367 \text{ cm}^{-1}$ , and  $\text{CH}_2$  bending at  $\sim 1439 \text{ cm}^{-1}$ . For gelatin, major peaks are found to be a C=O stretch at  $\sim 1645.2 \text{ cm}^{-1}$ , amide III at  $\sim 1036.9 \text{ cm}^{-1}$ ,  $\delta\text{-NH}$  or C-N stretch at  $\sim 1543.5 \text{ cm}^{-1}$ , -CO-NH-moiety at  $\sim 910.1 \text{ cm}^{-1}$ , C-O-C stretch at  $\sim 1363.4 \text{ cm}^{-1}$ , NH or OH stretch at  $\sim 3311.4 \text{ cm}^{-1}$ , and O-C-O symmetric stretch at  $\sim 1451.9 \text{ cm}^{-1}$  [40–50]. The rest of the modes are listed in Table A1 for readers' reference.

As the volumetric ratio of gelatin to PVA changes from pure gelatin (10:0) to pure PVA (0:10), the absorption peaks also change from gelatin's features to PVA's signatures. The most observable changes of peaks in Figure 9 due to mixing are the vanish peak at ( $2927 \text{ cm}^{-1}$  of CH  $\text{sp}^3$  in pure PVA)  $\rightarrow$  pure gelatin; ( $1728 \text{ cm}^{-1}$  of C=O in pure PVA)  $\rightarrow$  ( $1645 \text{ cm}^{-1}$  of C=O stretch in pure gelatin); the vanish peak at ( $1243.3 \text{ cm}^{-1}$  of C-O stretch in pure PVA)  $\rightarrow$  pure gelatin; the vanishing twin peaks ( $1025.5 \text{ cm}^{-1}$  of C-O stretch and C-O-C stretch of  $1090 \text{ cm}^{-1}$  in pure PVA)  $\rightarrow$  pure gelatin.

#### 4.2.4. Contact Angle

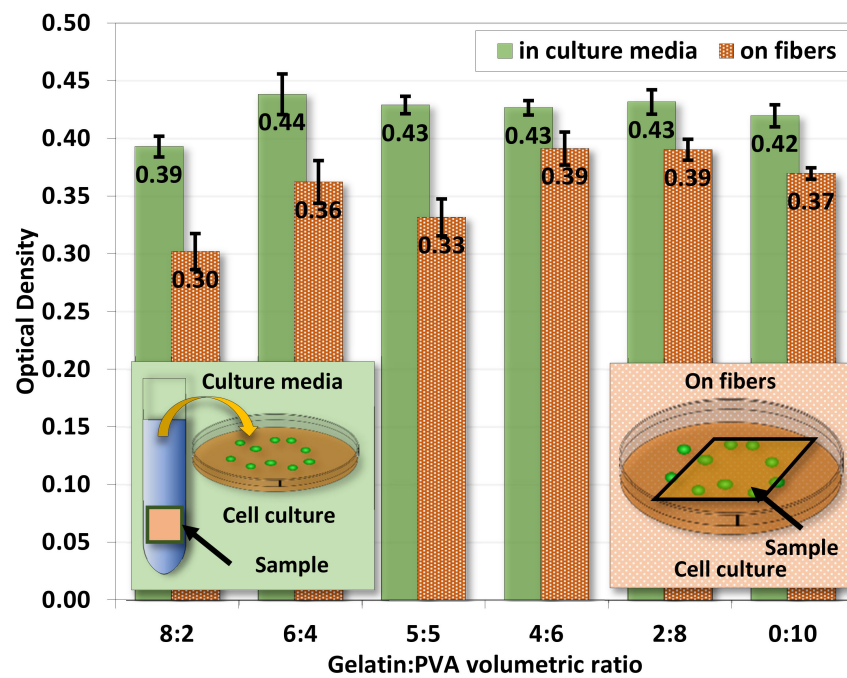
The averaged contact angles of gelatin/PVA fiber films are shown in Figure 10 where the time variation of the contact angle declines as the water drop is gradually absorbed into the fibers and films. There is a trend of such decreases corresponding to different compositions. When gelatin/PVA = 8:2, the contact angle decreases from 65° to 33° in about 105 s, while the opposite concentration, gelatin/PVA = 2:8, has the contact angle reduced from 65° to 40° in 150 s. The pure PVA is around the same variation of contact angle (55.3° to 40.67° in 150 s) close to that of the sample gelatin/PVA = 2:8. It seems that pure PVA, or PVA with a small amount of added gelatin, can sustain longer water dissolution as compared to the sample with a higher content of gelatin [53–57].



**Figure 10.** Water contact angle as a function of time for electrospun gelatin/PVA nanofiber films with different volumetric mixing ratios.

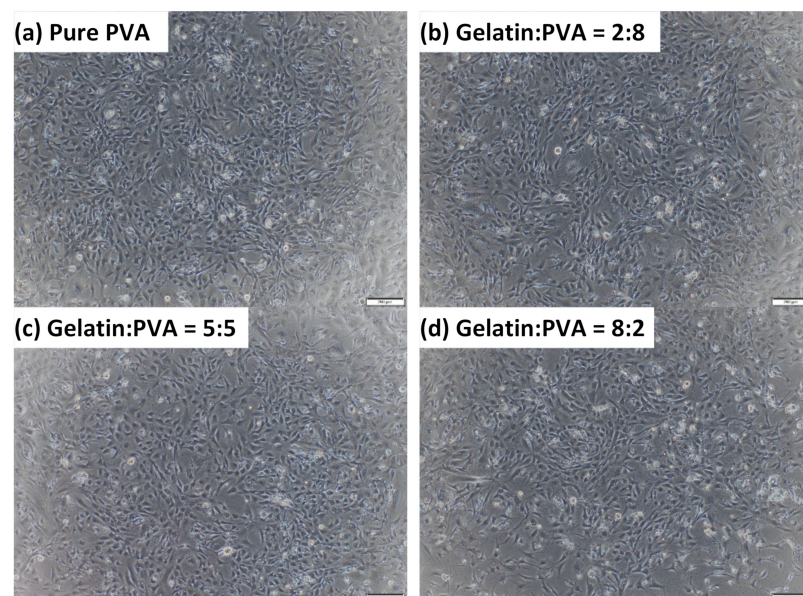
#### 4.3. Cell Culture

Figure 11 shows the ratio of optical densities from the MTT assay 48 h after 3T3 seeding in sample-immersed media and on fiber film samples. Both cases show comparable optical density in each sample whether 3T3 was cultured inside sample-immersed media or directly on samples. Overall, 3T3 directly cultured on samples has a lower optical density (cell count), and this is because cells are more likely to retain on samples. Samples of gelatin/PVA = 8:2 are slightly lower than others. This result provides evidence of non-toxic chemicals released from the gelatin/PVA fiber films from the 3T3 cell culture.



**Figure 11.** The average optical density from MTT assay for 3T3 cultured in culture media and on gelatin/PVA nanofiber films. The optical density is  $\log_{10} \left[ \frac{\text{incident light intensity}}{\text{transmitted light intensity}} \right]$ .

The morphologies of 3T3 at 48 h after seeding by an optical microscope are shown in Figure 12, where images are 3T3 in 24-well plates for fiber films of gelatin/PVA = 8:2, 5:5, 2:8, and 0:10 (pure PVA). We notice that although the optical density of the MTT assay for samples of gelatin/PVA = 8:2 is slightly lower, the morphologies of 3T3 present little difference from those cultured on other fiber films. Mostly, 3T3 cells in all cases can stretch and spread as in normal connective tissues ready for migration. This is an important indication of the non-toxic micro-environment in culture media derived from the gelatin/PVA fiber films.



**Figure 12.** Selected optical images (50 $\times$ ) of cultured 3T3 in media from immersed gelatin/PVA = 8:2, 5:5, 2:8, and pure PVA.

## 5. Discussion

### 5.1. Summary of Process Parameters for Electrospinning Nanofibers

Measurements on properties of gelatin/PVA polymeric solutions are meant to be an informative vindication for the possible formation of nanofibers by electrospinning. The regression models in Figures 2–5 provide estimates on the relationship between volumetric ratios of gelatin/PVA mixture and viscosity, electrical conductance, pH values, and surface tension, respectively. One simple way to examine the influence of different properties on the formation of nanofibers is to inspect the slope of regression functions. With the high fidelity of these fitting functions, i.e., all coefficients of determination  $R^2$  are greater than 0.95 (fitting model can explain or predict 95% of the variation of data) and narrow 95% confidence intervals of those coefficients in the fitting functions, the slope of the fitting function can represent the sensitivity of properties to different concentrations of gelatin/PVA. Table 3 compares sensitivities among all properties based on their regression functions. The most sensitive property to the varying concentrations of gelatin/PVA is found to be viscosity with a slope at least three orders larger than all other properties. The second one is the surface tension but with a negative slope. Both electrical conductance and pH value are only minimally affected by the concentrations of gelatin/PVA. Thus, the statistical inference from the data indicates that the formation of nanofibers by electrospinning is largely determined by the viscosity of the polymeric solution and surface tension, which suits the mechanisms of electrospinning [58–61]. It is particularly instructive for the case of pure PVA, whose relatively lower surface eases the stretching by the electrical field in electrospinning, but higher viscosity prevents overstretching beyond the Plateau–Rayleigh instability to become droplets.

**Table 3.** Statistical information of the fitting functions for the measurements of viscosity, electrical conductance, pH values, and surface tension of different gelatin/PVA mixed solutions.

	Volumetric Ratio Gel:PVA						
	10:0	8:2	6:4	5:5	4:6	2:8	0:10
<b>Viscosity</b>							
	$8.7258 \times e^{0.91109x}$						
Coefficient of Determination $R^2$	0.972						
95% confidence interval	$6.2662 \leq 8.7258 \leq 12.1508$ $0.8370 \leq 0.91109 \leq 0.9851$						
Sensitivity (slope of fitting function)	19.7542	49.1432	122.2549	304.1370	756.6103	1882.2410	4682.5044
<b>pH</b>							
	$y = 5.5143 \times 10^{-2}x + 3.232$						
Coefficient of Determination $R^2$	0.983						
95% confidence interval	$3.2088 \leq 3.232 \leq 3.2552$ $0.0492 \leq 0.055143 \leq 0.0611$						
Sensitivity (slope of fitting function)	0.0551						
<b>Electrical Conductance</b>							
	$y = -3.6419 \times 10^{-4}x + 2.7648 \times 10^{-3}$						
Coefficient of Determination $R^2$	0.966						
95% confidence interval	$0.0025 \leq 0.0027648 \leq 0.0030$ $-0.0003 \leq -0.00036419 \leq -0.0004$						
Sensitivity (slope of fitting function)	$-3.6419 \times 10^{-4}$						

Table 3. Cont.

	Volumetric Ratio Gel:PVA					
	10:0	8:2	6:4	5:5	4:6	2:8
	<b>Surface Tension</b>					
	$y = -1.0827x + 39.973$					
<b>Coefficient of Determination R<sup>2</sup></b>	0.982					
<b>95% confidence interval</b>	$39.2904 \leq 39.973 \leq 40.6562$ $-1.2354 \leq -1.0827 \leq -0.9300$					
<b>Sensitivity (slope of fitting function)</b>	-1.0827					

### 5.2. Fitting Model of Viscosity

Since viscosity is a dominant factor in the formation of nanofibers by electrospinning, a brief discussion on the viscosity is brought up herein. Since our polymeric solution is a mixture of two polymers, a blending of two viscosities should be expectable. Following the Lederer–Roegiers model for a binary mixture [62], the

$$\ln(\mu_{\text{mix}}) = \frac{x_{\text{gelatin}}}{x_{\text{gelatin}} + \alpha x_{\text{PVA}}} \ln(\mu_{\text{gelatin}}) + \frac{\alpha x_{\text{PVA}}}{x_{\text{gelatin}} + \alpha x_{\text{PVA}}} \ln(\mu_{\text{PVA}}) \quad (3)$$

where  $\mu_{\bullet}$  and  $x_{\bullet}$  are, respectively, the viscosity and molar fraction of either polymer.  $\alpha$  is an empirical constant.

One rough justification for these measurements is that when a solution has a viscosity higher than that of water its surface tension can be no higher than that of water (0.07275 J/m<sup>2</sup>). This is because higher surface tension is caused by intermolecular forces pulling surface molecules inwards, by which a local concentration gradient is created. This concentration gradient leads to a surface tension gradient which acts opposite to the movement. The interfacial movement is therefore damped.

Here is a reminder of earlier experimental results that the appropriate balance between higher viscosity ( $\sim 420\text{--}4300 \times 10^{-2}$  poise) and slightly lower surface tension ( $\sim 35.12\text{--}32.68$  mN/m<sup>2</sup>) of the mixed polymer solution would be favorable for the formation of nanofibers by our electrospinning system.

### 5.3. Estimation of the Interfacial Energy by Water Contact Test

The wettability by water contact in Figure 10 exhibits the spreading of water drops on the surface of nanofibers. A theoretical study on the spreading contact of a drop on a plane by M. Härth and D. W. Schubert provides an insightful view of the physics of an axisymmetric drop on partially and completely wetted substrates [63]. Considering a drop on the substrate as shown in Figure 13 the spreading of the drop is controlled by the balance among three forces, namely the capillary, gravity, and viscous friction on the interface between the drop and substrate, that is,

$$\underbrace{2\pi r \left( \Delta E + \gamma_L \frac{8V^2}{\pi^2 r^6} \right)}_{\text{Capillary Force}} + \underbrace{\frac{4\rho g V^2}{3\pi r^3}}_{\text{Gravitational Force}} - \underbrace{\frac{\eta r r^6}{\lambda' V^2}}_{\text{Viscous Friction Force}} = 0 \quad (4)$$

where  $r$ ,  $\rho$ ,  $V$ ,  $\eta$ , and  $\gamma_L$  are, respectively, the radius of the water contact circle on the substrate, the density, the total volume, the viscosity, and the surface tension (energy) of drop;  $g$  is the gravity constant;  $2\pi\lambda' \approx (37.1 \pm 14.1) \text{ m}^{-1}$  is a wetting-independent shape factor;  $s$  is the spreading parameter (penetration or seeping) as shown in Figure 13, and  $\dot{r} = \frac{dr}{dt}$  is the rate of spreading. The last remaining variable is the interfacial energy  $\Delta E$ ,

$$\Delta E = \gamma_S - \gamma_L - \gamma_{SL} \quad (5)$$

where  $\gamma$  is the surface energy (tension) with a subscript denoted for solid (S), liquid (L), or solid–liquid interface (SL). This is the unknown parameter subjected to the estimation discussed herein. Except for the surface energy of water surface energies  $\gamma_L$ , both  $\gamma_S$  (surface energy of nanofibers) and  $\gamma_{SL}$  (interfacial energy between nanofibers and water) are unknown.  $\gamma_S$  may be roughly estimated from the solid PVA and gelatin, but faithful values of  $\gamma_{SL}$  are unfound in the literature. In fact,  $\gamma_L$  and  $\gamma_S$  have their unique values because of the dependence on their respect morphologies and chemical compositions.

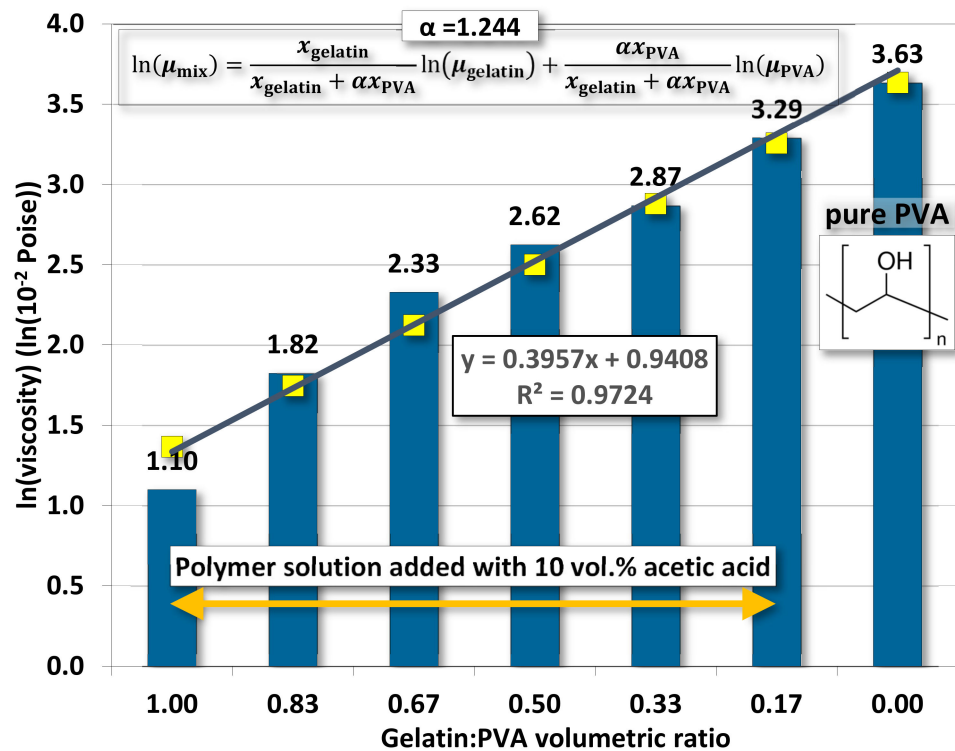


**Figure 13.** A mixture model for fitting the viscosity of gelatin/PVA mixed solutions. The empirical coefficient  $\alpha$  is obtained by minimizing errors in the  $L^2$  norm (square root of the sum of error<sup>2</sup>) between experimental data and fitting numbers.

Experimentally,  $r$  and  $h$  can be measured from the image of the drop. Then, the radius  $R$  and spreading parameter  $s$  of a partially wetting drop are determined by the following geometric relation (cf. Figure 14):

$$s + h = R \tag{6}$$

$$r^2 + s^2 = R^2 \tag{7}$$

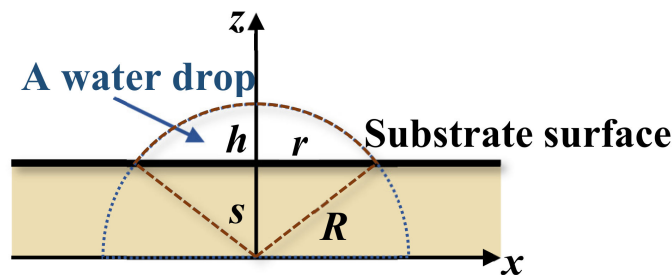


**Figure 14.** A schematic drawing of a drop of liquid on a partially wetted substrate.

Therefore,

$$R = \frac{h}{2} \left( \left( \frac{r}{h} \right)^2 + 1 \right) \tag{8}$$

$$s = \frac{h}{2} \left( \left( \frac{r}{h} \right)^2 - 1 \right) \quad (9)$$

To solve equation (4) we first define a new variable,

$$u = r^6 \quad (10)$$

Dividing (4) by  $2\pi r$  on both sides, we then have

$$\frac{\eta \dot{r} r^5}{2\pi \lambda V^2} = \left( \Delta E + \gamma_L \frac{8V^2}{\pi^2 r^6} \right) + \frac{2\rho g V^2}{3\pi^2 r^4} \quad (11)$$

where  $\lambda = 2\pi \lambda' \approx (37.1 \pm 14.1) \text{ m}^{-1}$  [63]. The initial condition for this non-linear ordinary differential equation is

$$u(0) = r^6(0) \quad (12)$$

This condition represents the initial spherical drop in contact with the substrate. Practically, in most experiments of contact angle cases, the initial condition should start with a finite contact width  $r_0$ ; therefore, the initial condition is

$$u(0) = (r(0))^6 = (r_0)^6 \quad (13)$$

We used this condition for the following numerical analysis. The steps to determine the surface energy  $\Delta E$  are:

- We first determine  $r$  and  $h$  at the selected time (including initial values of  $r_0$  and  $h_0$ ) from the image of the water drop for the contact angle test;
- Radius of the drop  $R$  and penetration  $s$  can be calculated following Equations (8) and (9). Then, the volume of the drop can be calculated by simple integration shown in Appendix A;
- For water at 25 °C, the surface tension of  $\gamma_L = 0.07275 \text{ J/m}^2$ , viscosity is 0.0091, and poise and density are  $997 \text{ kg/m}^3$ ;
- The rate change,  $\dot{r}$ , is estimated from the fitting functions, as shown in Figure 15;
- The interfacial energy  $\Delta E$  at different times is estimated from Equation (11) as

$$\Delta E = \frac{\eta \dot{r} r^5}{2\pi \lambda V^2} - \gamma_L \frac{8V^2}{\pi^2 r^6} - \frac{2\rho g V^2}{3\pi^2 r^4} \quad (14)$$

- Plugging values of  $\Delta E$  at each time back to eq. (11) to re-calculate  $\dot{r}$ . These  $\dot{r}$  are different from the  $\dot{r}$  estimated from the fitting functions;
- Among various values of  $\Delta E$  at each time, an optimal value that minimizes the difference of  $\dot{r}$  between the fitting function and the previous step can be determined accordingly.

Figure 15 shows the variation of width  $r$  of water drops at different times for different gelatin/PVA concentrations. As time elapsed, the drop gradually flattens as  $r$  increases. Using the procedure just mentioned, the estimated interfacial energies  $\Delta E$  for different compositions of nanofibers are shown in Figure 16. The optimal estimate of  $\Delta E$  in the range between  $\sim -0.028$  and  $\sim -0.059 \text{ J/m}^2$  is found for different nanofibers. The negative values of  $\Delta E$  confirm the partial wetting regime as indicated in [63]. If considering the surface energy of pure water at 25 °C and  $\gamma_L \approx 0.72 \text{ J/m}^2$ , the pure gelatin or pure PVA  $\gamma_S \approx 0.033\text{--}0.29 \text{ J/m}^2$  [64–66] and then the interfacial  $\gamma_{SL} = (\gamma_S - \gamma_L - \Delta E)$  would be approximately  $(-0.0259\text{--}0.2311 \text{ J/m}^2)$  and  $(-0.0146\text{--}0.2424 \text{ J/m}^2)$ . The negative values are physically infeasible as the interface between nanofibers and water becomes unstable. Since there is a lack of data in the literature, these values are referential for further investigations.

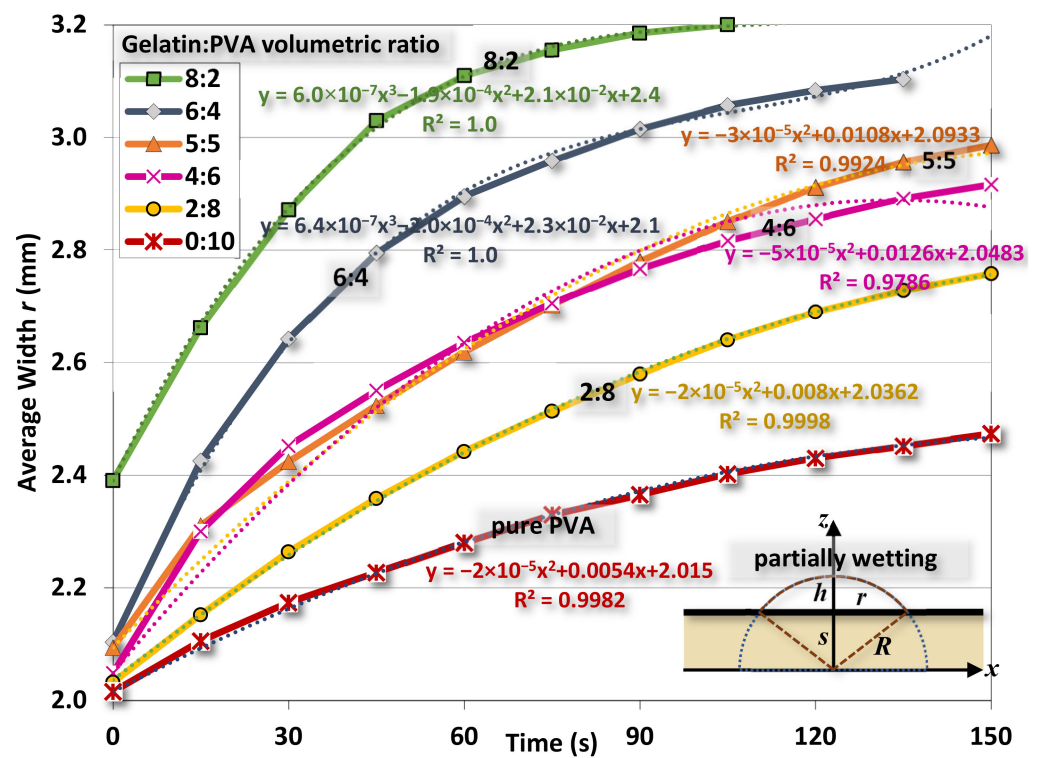


Figure 15. Variations of the width  $r$  of water contact as functions of time.

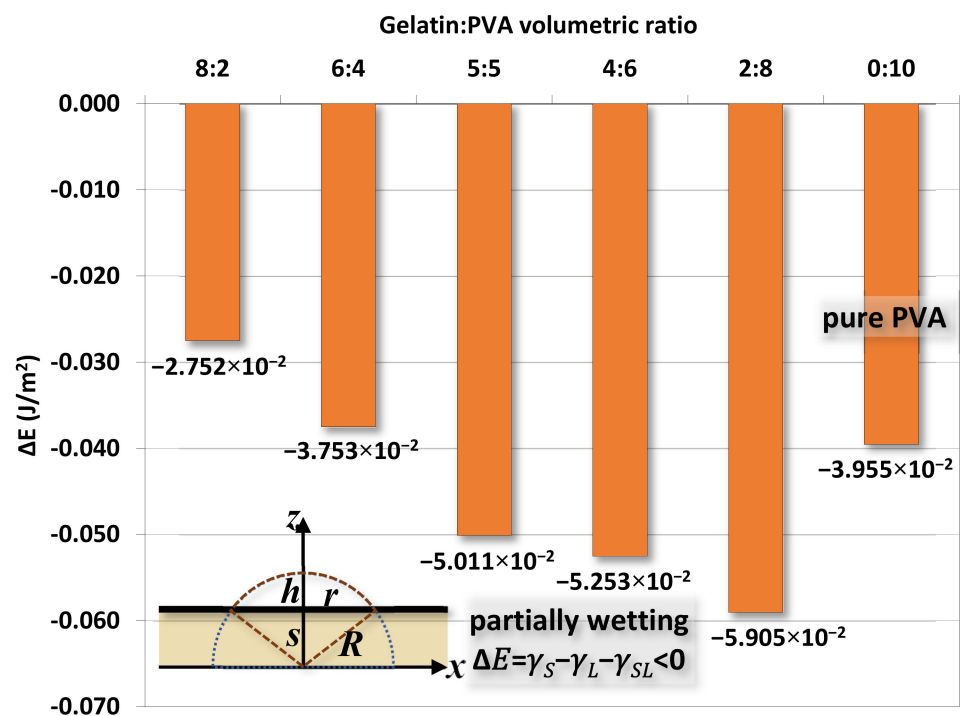


Figure 16. The optimal estimate of interfacial energy  $\Delta E$  from the width  $r$  of water contact and model proposed by Härth and Schubert.

### 6. Conclusions

In this study, we investigated the relationship between the compositions of gelatin/PVA mixed hydrogels and the electrospinning process. The electrospun gelatin nanofibers mixed with different concentrations of PVA were deposited on a layer film of the same compositions by spin coating. An important point is to determine a window of composition for

the successful fabrication of nanofibers. The investigation was conducted twofold. One front was to measure the properties of polymer solutions including viscosity, pH value, electrical conductance, and surface tension. Another side was to analyze the compositions and properties of nanofibers by FTIR, SEM, and EDS. For the polymer solutions, we found that viscosity is a dominant factor influencing the formation of nanofibers, and surface tension is a secondary factor. The pH value and electrical conductance are only marginal factors. The FTIR confirms that gelatin and PVA are physically miscible during the formation of nanofibers with the support of surface elemental analysis by EDS and SEM images of nanofibers. The hydrophilicity of nanofibers was tested by water contact angle at a prolonged period. As time expands, water drops gradually flattened as an indication of becoming more hydrophilic. We specifically introduced a theoretical model by Härth and Schubert for the spread of water contact to estimate the interfacial surface energy between the water drop and nanofibers. A range of  $-0.02752$ – $0.2763$  J/m<sup>2</sup> was predicted for the mixed gelatin/PVA nanofibers. In addition to the material characterizations, specially chosen gelatin/PVA nanofiber samples were tested for their biotoxicity via the cell culture of 3T3 fibroblasts. Both optical images and MTT assays show that 3T3 spreads and proliferates healthily after 48 h of seeding without signs of necrosis.

**Author Contributions:** H.Y.C. and N.Y.C.: experiment, formal analysis, investigation, software, data curation, and visualization. C.L.: conceptualization, methodology (fabrication and characterizations), software, writing (original draft), supervision, and project administration. V.C.: conceptualization, methodology (biochemical analysis), writing (review and editing), validation, and resources. J.H.H.: conceptualization, methodology (materials), resources, supervision, and writing (review and editing). Y.-H.T.: investigation, resources (cell culture), and funding acquisition. T.L.: resources and funding acquisition. All authors have read and agreed to the published version of the manuscript.

**Funding:** This research was funded by the NYCU–Far Eastern Memorial Hospital Joint Research Program, grant number 110DN08, and the NYCU–Cheng Hsin General Hospital Joint Research Program, grant number CY11010.

**Institutional Review Board Statement:** Not applicable.

**Informed Consent Statement:** Not applicable.

**Data Availability Statement:** The data presented in this study are available on request from the corresponding author.

**Conflicts of Interest:** The authors declare no conflict of interest.

## Appendix A. Integration of Drop Volume in the Contact Angle Test

The volume of the water drop in the contact angle test can be calculated by simple integration. Assuming axisymmetry of the drop along the z-axis in Figure 12, the drop volume  $V$  is

$$\int_s^R \pi r^2 dz = \int_s^R \pi (R^2 - z^2) dz = \pi \left( \frac{2}{3} R^3 - (R^2 s) - \frac{1}{3} s^3 \right) \quad (\text{A1})$$

## Appendix B. Major FTIR Absorption Peaks

Some FTIR absorption peaks are listed in Table A1 for readers' reference.

**Table A1.** Major FTIR absorption peaks for gelatin and PVA [40–50].

Wavenumber (cm <sup>-1</sup> )	Gelatin Mode	Reference
400–900	–CO–NH–moiety, amide IV–VI bands	[41]
670–1240	Amide III (C–N, in-plane bending vibrations of N–H, weak C–C bond, and C=O)	[43]
900–1900	Amide I, II, and III	[41]
1238	Delta N–H, C–N stretching	[40]

Table A1. Cont.

Wavenumber (cm <sup>-1</sup> )	Gelatin Mode	Reference
1245	Amide III	[44]
1300–1560	Amide II (N-H bond-bending mode and stretching vibration of C-N bond)	[43]
1328	Wagging vibration of proline side chains	[42]
1400	Symmetric O–C–O stretching	[40]
1500–1550	N-H deformation	[42]
1540	Amide II	[42]
1541	Delta N-H, C-N stretching	[40]
1560	Amide II	[44]
1620–1660	Amide I (stretching of carbonyl C=O (peptide bond) with less involvement of the stretching C-N bond)	[43]
1637	C=O stretching	[42]
1650	Amide I	[44]
1653	C=O, CN stretching	[40]
2300–3600	Amide A	[43]
2700–3600	Amide A and B	[41]
2947	C-H stretching	[42]
2960–2935	Asymmetric and symmetric CH <sub>2</sub> stretching	[40]
3065	N-H stretching	[40]
3270–3370	N-H stretching	[42]
3306	N-H, O-H stretching	[40]
Wavenumber (cm <sup>-1</sup> )	PVA Mode	Reference
839	C-C stretching vibration	[48]
849	C-H rocking mode	[50]
1000–1100	C–O stretching in C–O–H groups and COC groups	[50]
1081	C–O stretching of acetyl groups	[48]
1085–1150	C–O–C	[47]
1100	C–O–C	[45]
1140	Crystalline C–O stretching	[50]
1141	C–O (crystallinity)	[47]
1248	C–O stretching	[50]
1261	C–O stretching	[50]
1324	C–H deformation vibration	[48]
1377	CH <sub>3</sub> bending	[45]
1417–1461	Delta CH <sub>2</sub>	[47]
1425	C–H bending vibration of CH <sub>2</sub>	[48]
1435	C–H bending	[50]
1440	CH <sub>2</sub> bending	[45]
1680–1730	C=O and C–O stretch from the remaining acetate groups	[46]
1690	C=O carbonyl stretch	[48]
1720–1737	C=O stretching	[45]
1732	C=O stretching	[50]
1735–1750	C=O	[47]
2840	Symmetric stretching vibrational of C–H from alkyl groups	[49]
2840–3000	C-H stretch from alkyl groups	[46]
2914	C–H stretching from the alkyl groups	[50]
2917	CH <sub>2</sub> asymmetric stretching	[48]
2920	Antisymmetric stretching vibrational of C–H from alkyl groups	[49]
2929	CH sp <sup>3</sup>	[45]
2943	C–H stretching from the alkyl groups	[50]

Table A1. Cont.

Wavenumber (cm <sup>-1</sup> )	Gelatin Mode	Reference
3200–3550	O-H stretching	[46]
3280	O-H stretching	[48]
3369	O-H stretching	[50]
3400	O-H stretching	[49]
3411	O-H stretching	[45]

## References

- Sousa Coelho, D.; Veleirinho, B.; Alberti, T.; Maestri, A.; Yunes, R.; Dias, P.; Maraschin, M. Electrospinning Technology: Designing Nanofibers toward Wound Healing Application. In *Nanomaterials—Toxicity, Human Health and Environment*; Clichici, S., Filip, A., M. do Nascimento, G., Eds.; IntechOpen: London, UK, 2018.
- Samadian, H.; Zamiri, S.; Ehterami, A.; Farzamfar, S.; Vaez, A.; Khastar, H.; Alam, M.; Ai, A.; Derakhshankhah, H.; Allahyari, Z.; et al. Electrospun cellulose acetate/gelatin nanofibrous wound dressing containing berberine for diabetic foot ulcer healing: In vitro and in vivo studies. *Sci. Rep.* **2020**, *10*, 8312. [\[CrossRef\]](#)
- Liu, X.; Xu, H.; Zhang, M.; Yu, D.-G. Electrospun medicated nanofibers for wound healing: Review. *Membranes* **2021**, *11*, 770. [\[CrossRef\]](#)
- Liu, Y.; Zhou, S.; Gao, Y.; Zhai, Y. Electrospun nanofibers as a wound dressing for treating diabetic foot ulcer. *J. Pharm. Sci.* **2019**, *14*, 130–143. [\[CrossRef\]](#) [\[PubMed\]](#)
- Ng, C.; Hamzah, M.; Razak, S.I.A.; Sukor, J.; Nayan, N.; Hasraf, N. Study on morphological properties of polyvinyl alcohol/poly(lactic acid) wound dressing membrane as drug delivery carrier in wound healing treatment. *J. Adv. Manuf. Technol.* **2020**, *1*, 7–11. [\[CrossRef\]](#)
- Pilehvar-Soltanahmadi, Y.; Dadashpour, M.; Mohajeri, A.; Fattahi, A.; Sheervalilou, R.; Zarghami, N. An overview on application of natural substances incorporated with electrospun nanofibrous scaffolds to development of innovative wound dressings. *Mini-Rev. Med. Chem.* **2018**, *18*, 414–427. [\[CrossRef\]](#) [\[PubMed\]](#)
- Mousavi, S.-M.; Nejad, Z.M.; Hashemi, S.A.; Salari, M.; Gholami, A.; Ramakrishna, S.; Chiang, W.-H.; Lai, C.W. Bioactive agent-loaded electrospun nanofiber membranes for accelerating healing process: A review. *Membranes* **2021**, *11*, 702. [\[CrossRef\]](#)
- Arampatzis, A.S.; Kontogiannopoulos, K.N.; Theodoridis, K.; Aggelidou, E.; Rat, A.; Willems, A.; Tsivintzelis, I.; Papageorgiou, V.P.; Kritis, A.; Assimopoulou, A.N. Electrospun wound dressings containing bioactive natural products: Physico-chemical characterization and biological assessment. *Biomater. Res.* **2021**, *25*, 23. [\[CrossRef\]](#) [\[PubMed\]](#)
- Namekawa, K.; Schreiber, M.T.; Aoyagia, T.; Ebara, M. Fabrication of zeolite-polymer composite nanofibers for removal of uremic toxins from kidney failure patients. *Biomater. Sci.* **2014**, *2*, 674–679. [\[CrossRef\]](#)
- Subtirica, A.I.; Banciu, C.A.; Chivu, A.A.M.; Dinca, L.C. Nanofibres made from biocompatible and biodegradable polymers, with potential application as medical textiles. *Ind. Text.* **2018**, *69*, 55–58.
- Güler, B. Comparative analysis of superabsorbent properties of PVP and PAA nanofibers. *Ind. Text.* **2021**, *72*, 460–466. [\[CrossRef\]](#)
- Raja, I.S.; Preeth, D.R.; Vedhanayagam, M.; Hyon, S.-H.; Lim, D.; Kim, B.; Rajalakshmi, S.; Han, D.-W. Polyphenols-loaded electrospun nanofibers in bone tissue engineering and regeneration. *Biomater. Res.* **2021**, *25*, 29. [\[CrossRef\]](#) [\[PubMed\]](#)
- Sheikh, F.A.; Ju, H.W.; Lee, J.M.; Moon, B.M.; Park, H.J.; Lee, O.J.; Kim, J.-H.; Kim, D.-K.; Park, C.H. 3D electrospun silk fibroin nanofibers for fabrication of artificial skin. *Nanomed. Nanotechnol. Biol. Med.* **2015**, *11*, 681–691. [\[CrossRef\]](#) [\[PubMed\]](#)
- Tan, H.; Marra, K.G. Injectable, biodegradable hydrogels for tissue engineering applications. *Materials* **2010**, *3*, 1746–1767. [\[CrossRef\]](#)
- Lee, J.H. Injectable hydrogels delivering therapeutic agents for disease treatment and tissue engineering. *Biomater. Res.* **2018**, *22*, 27. [\[CrossRef\]](#)
- Liu, M.; Zeng, X.; Ma, C.; Yi, H.; Ali, Z.; Mou, X.; Li, S.; Deng, Y.; He, N. Injectable hydrogels for cartilage and bone tissue engineering. *Bone Res.* **2017**, *5*, 17014. [\[CrossRef\]](#)
- Cook, M.T.; Smith, S.L.; Khutoryanskiy, V.V. Novel glycopolymer hydrogels as mucosa-mimetic materials to reduce animal testing. *Chem. Comm.* **2015**, *51*, 14447–14450. [\[CrossRef\]](#) [\[PubMed\]](#)
- Al-Nimry, S.; Dayah, A.A.; Hasan, I.; Daghmash, R. Cosmetic, biomedical and pharmaceutical applications of fish gelatin/hydrolysates. *Mar. Drugs* **2021**, *19*, 145. [\[CrossRef\]](#)
- Schmidt, M.M.; Prestes-Dornelles, R.; Mello, R.; Kubota, E.H.; Mazutti, M.; Kempka, A.; Demiate, I. Collagen extraction process. *Int. Food Res. J.* **2016**, *23*, 913–922.
- Mokrejs, P.; Langmaier, F.; Mladek, M.; Janacova, D.; Kolomaznik, K.; Vasek, V. Extraction of collagen and gelatine from meat industry by-products for food and non food uses. *Waste Manag. Res.* **2009**, *27*, 31–37. [\[CrossRef\]](#)
- Ahmad, T.; Ismail, A.; Ahmad, S.A.; Abdul Khalil, K.; Awad, E.A.; Akhtar, M.T.; Sazili, A.Q. Recovery of gelatin from bovine skin with the aid of pepsin and its effects on the characteristics of the extracted gelatin. *Polymers* **2021**, *13*, 1554. [\[CrossRef\]](#)
- Sompie, M.; Surtijono, S.E.; Pontoh, J.H.W.; Lontaan, N.N. The effects of acetic acid concentration and extraction temperature on physical and chemical properties of pigskin gelatin. *Procedia Food Sci.* **2015**, *3*, 383–388. [\[CrossRef\]](#)
- Kariduraganavar, M.Y.; Kittur, A.A.; Kamble, R.R. Chapter 1—Polymer Synthesis and Processing. In *Natural and Synthetic Biomedical Polymers*; Kumbar, S.G., Laurencin, C.T., Deng, M., Eds.; Elsevier: Oxford, UK, 2014; pp. 1–31.

24. Arsyanti, L.; Erwanto, Y.; Rohman, A.; Pranoto, Y. Chemical composition and characterization of skin gelatin from buffalo (*Bubalus bubalis*). *Int. Food Res. J.* **2018**, *25*, 1095–1099.
25. Eastoe, J.E. The amino acid composition of mammalian collagen and gelatin. *Biochem. J.* **1955**, *61*, 589–600. [[CrossRef](#)]
26. Siregar, G.R.M.; Suprayitno, E. Amino acid composition of gelatin from ephinephelus sp. *J. Agric. Vet. Sci.* **2019**, *12*, 51–54.
27. Duconseille, A.; Astruc, T.; Quintana, N.; Meersman, F.; Sante-Lhoutellier, V. Gelatin structure and composition linked to hard capsule dissolution: A review. *Food Hydrocoll.* **2015**, *43*, 360–376. [[CrossRef](#)]
28. Ali, E.; Sultana, S.; Hamid, S.B.A.; Hossain, M.; Yehya, W.A.; Kader, A.; Bhargava, S.K. Gelatin controversies in food, pharmaceuticals, and personal care products: Authentication methods, current status, and future challenges. *Crit. Rev. Food Sci. Nutr.* **2018**, *58*, 1495–1511. [[CrossRef](#)] [[PubMed](#)]
29. Said, M. Role and function of gelatin in the development of the food and non-food industry: A review. *IOP Conf. Ser. Earth Environ. Sci.* **2020**, *492*, 012086. [[CrossRef](#)]
30. Nitsuwat, S.; Zhang, P.; Ng, K.; Fang, Z. Fish gelatin as an alternative to mammalian gelatin for food industry: A meta-analysis. *LWT* **2021**, *141*, 110899. [[CrossRef](#)]
31. Liang, M.; Li, Z.; Gao, C.; Wang, F.; Chen, Z. Preparation and characterization of gelatin/sericin/carboxymethyl chitosan medical tissue glue. *J. Appl. Biomater. Funct. Mater.* **2018**, *16*, 97–106. [[CrossRef](#)]
32. Zhang, L.; Zhou, Y.; Wu, Q.; Han, Z.; Zhao, Z.; Li, F.; Wang, C.; Wei, K.; Li, G. A functional polyvinyl alcohol fibrous membrane loaded with artemisinin and chloroquine phosphate. *J. Polym. Res.* **2021**, *28*, 232. [[CrossRef](#)]
33. Baker, M.I.; Walsh, S.P.; Schwartz, Z.; Boyan, B.D. A review of polyvinyl alcohol and its uses in cartilage and orthopedic applications. *J. Biomed. Mater. Res. Part B Appl. Biomater.* **2012**, *100*, 1451–1457. [[CrossRef](#)] [[PubMed](#)]
34. Teodorescu, M.; Bercea, M.; Morariu, S. Biomaterials of PVA and PVP in medical and pharmaceutical applications: Perspectives and challenges. *Biotechnol. Adv.* **2019**, *37*, 109–131. [[CrossRef](#)] [[PubMed](#)]
35. Feldman, D. Poly(Vinyl Alcohol) recent contributions to engineering and medicine. *J. Compos. Sci.* **2020**, *4*, 175. [[CrossRef](#)]
36. Muppalaneni, S. Polyvinyl alcohol in medicine and pharmacy: A perspective. *J. Dev. Drugs* **2013**, *02*. [[CrossRef](#)]
37. National Toxicology Program. Available online: <https://ntp.niehs.nih.gov/> (accessed on 28 April 2022).
38. Quan, L.; Xin, Y.; Wu, X.; Ao, Q. Mechanism of Self-Healing Hydrogels and Application in Tissue Engineering. *Polymers* **2022**, *14*, 2184. [[CrossRef](#)] [[PubMed](#)]
39. Mad-Ali, S.; Benjakul, S.; Prodpran, T.; Maqsood, S. Characteristics and gelling properties of gelatin from goat skin as affected by drying methods. *J. Food Sci. Technol.* **2017**, *54*, 1646–1654. [[CrossRef](#)]
40. Derkach, S.R.; Voron'ko, N.G.; Sokolan, N.I.; Kolotova, D.S.; Kuchina, Y.A. Interactions between gelatin and sodium alginate: UV and FTIR studies. *J. Dispers. Sci. Technol.* **2020**, *41*, 690–698. [[CrossRef](#)]
41. Saidi, G.; Rahman, M.; Guizani, N. Fourier transform infrared (FTIR) spectroscopic study of extracted gelatin from shaari (*Lithrinus microdon*) skin: Effects of extraction conditions. *Int. Food Res. J.* **2012**, *19*, 1167–1173.
42. Qadir, M.; Hossain, J.; Gafur, M.; Karim, M. Preparation and characterization of gelatin-hydroxyapatite composite for bone tissue engineering. *Int. J. Eng. Sci.* **2014**, *14*, 24.
43. Irfanita, N.; Jaswir, I.; Mirghani, M.; Sukmasari, S.; Dewi Ardini, Y.; Lestari, W. Rapid detection of gelatin in dental materials using attenuated total reflection Fourier transform infrared spectroscopy (ATR-FTIR). *J. Phys. Conf. Ser.* **2017**, *884*, 012090. [[CrossRef](#)]
44. Payne, K.J.; Veis, A. Fourier transform infrared spectroscopy of collagen and gelatin solutions: Deconvolution of the amide I band for conformational studies. *Biopolymers* **1988**, *27*, 1749–1760. [[CrossRef](#)]
45. Hendrawan, H.; Khoerunnisa, F.; Sonjaya, Y.; Putri, A.D. Poly (vinyl alcohol)/glutaraldehyde/*Premna oblongifolia* merr extract hydrogel for controlled-release and water absorption application. *IOP Conf. Ser. Mater. Sci. Eng.* **2019**, *509*, 012048. [[CrossRef](#)]
46. Alhosseini, S.N.; Moztarzadeh, F.; Mozafari, M.; Asgari, S.; Dodel, M.; Samadikuchaksaraei, A.; Kargozar, S.; Jalali, N. Synthesis and characterization of electrospun polyvinyl alcohol nanofibrous scaffolds modified by blending with chitosan for neural tissue engineering. *Int. J. Nanomed.* **2012**, *7*, 25–34.
47. Mansur, H.S.; Sadahira, C.M.; Souza, A.N.; Mansur, A.A.P. FTIR spectroscopy characterization of poly (vinyl alcohol) hydrogel with different hydrolysis degree and chemically crosslinked with glutaraldehyde. *Mater. Sci. Eng. C* **2008**, *28*, 539–548. [[CrossRef](#)]
48. Kharazmi, A.; Faraji, N.; Mat Hussin, R.; Saion, E.; Yunus, W.M.; Behzad, K. Structural, optical, opto-thermal and thermal properties of ZnS-PVA nanofluids synthesized through a radiolytic approach. *Beilstein J. Nanotechnol.* **2015**, *6*, 529–536. [[CrossRef](#)] [[PubMed](#)]
49. Awada, H.; Daneault, C. Chemical modification of poly(vinyl alcohol) in water. *Appl. Sci.* **2015**, *5*, 840–850. [[CrossRef](#)]
50. Lin, S.-Y.; Cheng, W.-T.; Wei, Y.-S.; Lin, H.-L. DSC-FTIR microspectroscopy used to investigate the heat-induced intramolecular cyclic anhydride formation between Eudragit E and PVA copolymer. *Polym. J.* **2011**, *43*, 577–580. [[CrossRef](#)]
51. Liu, B.; Zhang, J.; Guo, H. Research progress of polyvinyl alcohol water-resistant film materials. *Membranes* **2022**, *12*, 347. [[CrossRef](#)] [[PubMed](#)]
52. Bahram, M.; Mohseni, N.; Moghtader, M. An introduction to hydrogels and some recent applications. In *Emerging Concepts in Analysis and Applications of Hydrogels*; Majee, S., Ed.; IntechOpen: London, UK, 2016.
53. Kobayashi, M.; Kanekiyo, M.; Ando, I.; Amiya, S. A study of the gelation mechanism of poly(vinyl alcohol) in aqueous solution by high-resolution solid-state <sup>13</sup>C NMR spectroscopy. *Polym. Gels Netw.* **1998**, *6*, 425–428. [[CrossRef](#)]
54. Takeshita, H.; Kanaya, T.; Nishida, K.; Kaji, K. Gelation process and phase separation of PVA solutions as studied by a light scattering technique. *Macromolecules* **1999**, *32*, 7815–7819. [[CrossRef](#)]

55. Bercea, M.; Morariu, S.; Rusu, D. In situ gelation of aqueous solutions of entangled poly(vinyl alcohol). *Soft Matter* **2013**, *9*, 1244–1253. [[CrossRef](#)]
56. Kanaya, T.; Takahashi, N.; Takeshita, H.; Ohkura, M.; Nishida, K.; Kaji, K. Structure and dynamics of poly(vinyl alcohol) gels in mixtures of dimethyl sulfoxide and water. *Polym. J.* **2012**, *44*, 83–94. [[CrossRef](#)]
57. Cavalieri, F.; Miano, F.; D'Antona, P.; Paradossi, G. Study of gelling behavior of poly(vinyl alcohol)-methacrylate for potential utilizations in tissue replacement and drug delivery. *Biomacromolecules* **2004**, *5*, 2439–2446. [[CrossRef](#)]
58. Hetsroni, G.; Zakin, J.L.; Lin, Z.; Mosyak, A.; Pancallo, E.A.; Rozenblit, R. The effect of surfactants on bubble growth, wall thermal patterns and heat transfer in pool boiling. *Int. J. Heat Mass Transf.* **2001**, *44*, 485–497. [[CrossRef](#)]
59. Yang, Q.; Li, Z.; Hong, Y.; Zhao, Y.; Qiu, S.; Wang, C.; Wei, Y. Influence of solvents on the formation of ultrathin uniform poly(vinyl pyrrolidone) nanofibers with electrospinning. *J. Polym. Sci. B Polym. Phys.* **2004**, *42*, 3721–3726. [[CrossRef](#)]
60. Prahasti, G.; Zulfi, A.; Munir, M.M. Needleless electrospinning system with wire spinneret: An alternative way to control morphology, size, and productivity of nanofibers. *Nano Express* **2020**, *1*, 010046. [[CrossRef](#)]
61. Ahmmed, K.M.T.; Syeda, S. Enhancement of nucleate pool boiling heat transfer with sodium oleate. *J. Chem. Eng.* **2017**, *29*, 44. [[CrossRef](#)]
62. Zhmud, B. Viscosity Blending Equations. *Lube* **2014**, *121*, 24.
63. Härth, M.; Schubert, D.W. Simple approach for spreading dynamics of polymeric fluids. *Macromol. Chem. Phys.* **2012**, *213*, 654–665. [[CrossRef](#)]
64. Kuo, T.-Y.; Jhang, C.-F.; Lin, C.-M.; Hsien, T.-Y.; Hsieh, H.-J. Fabrication and application of coaxial poly(vinyl alcohol)/chitosan nanofiber membranes. *Open Phys. J.* **2017**, *15*, 1004–1014. [[CrossRef](#)]
65. Bhattacharya, A.; Ray, P. Studies on surface tension of poly(vinyl alcohol): Effect of concentration, temperature, and addition of chaotropic agents. *J. Appl. Polym. Sci.* **2004**, *93*, 122–130. [[CrossRef](#)]
66. Johnston, J.H.; Peard, G.T. The surface tension of gelatin solutions. *Biochem. J.* **1925**, *19*, 281–289. [[CrossRef](#)] [[PubMed](#)]